Visual Features as Carriers of Abstract Quantitative Information

Ronald A. Rensink

Departments of Computer Science and Psychology
University of British Columbia, Vancouver, Canada

Journal of Experimental Psychology: General, **151**(8): 1793-1820. doi.org/10.1037/xge0001165

Author Notes

Ronald A. Rensink, Departments of Psychology and Computer Science, University of British Columbia.

This work was supported in part by a grant from The Boeing Company. Many thanks to Akbar Alikhan, Jason Chang, Jessie Chen, Jacky Chung, Mario Cimet, Emily Hindalong, Jessica Ip, Adelena Leon, Alex Miszkurka, Praveena Manogaran, Hae Jung Min, Yana Pertels, Ramyar Sigarchy, Kristen Waterman, Spencer Williams, and Eric Wong for their immense effort in data collection and preliminary analysis, and to Madison Elliott and Amon Ge for help with programming. Thanks also to the editor, an anonymous reviewer, and Jeremy Wolfe for their feedback on earlier versions of the paper. Part of the data here was presented at the 2015 Vision Sciences Society conference in St. Petersburg, FL, USA, and at the 2017 European Conference on Visual Perception in Berlin, Germany.

None of the experiments were formally preregistered. The data and materials for all experiments are available at https://osf.io/2wgb7, or upon request.

Correspondence concerning this article should be addressed to Ronald A. Rensink, Department of Psychology, University of British Columbia, 2136 West Mall, Vancouver, BC, Canada, V6T 1Z4. Email: rensink@psych.ubc.ca.

Version: November 3, 2021

Word count: 15,971

Abstract

Four experiments investigated the extent to which abstract quantitative information can be conveyed by basic visual features. This was done by asking observers to estimate and discriminate Pearson correlation in graphical representations where the first data dimension of each element was encoded by its horizontal position, and the second by the value of one of its visual features; perceiving correlation then requires combining the information in the two encodings via a common abstract representation. Four visual features were examined: luminance, color, orientation, and size. All were able to support the perception of correlation. Indeed, despite the strikingly different appearances of the associated stimuli, all gave rise to performance that was much the same: just noticeable difference was a linear function of distance from complete correlation, and estimated correlation a logarithmic function of this distance. Performance differed only in regards to the level of noise in the feature, with these values compatible with estimates of channel capacity encountered in classic experiments on absolute perceptual magnitudes. These results suggest that quantitative information can be conveyed by visual features that are abstracted at relatively low levels of visual processing, with little representation of the original sensory property. It is proposed that this is achieved via an abstract parameter space in which the values in each perceptual dimension are normalized to have the same means and variances, with perceived correlation based on the shape of the joint probability density function of the resultant elements.

Visual Features as Carriers of Abstract Quantitative Information

The area of information visualization concerns itself with the effective display of information in graphical form (e.g., Spence, 2014; Ware, 2012). Here, physical properties such as color and orientation—often referred to as *visual variables* (Bertin, 1967/2011)—are used for four purposes: (i) forming spatial groups, (ii) creating items that are visually distinct, (iii) facilitating attentional selection of sets of items, and (iv) encoding quantitative information (Card, Mackinlay, & Shneiderman, 1999; Roth, 2017).[1] The perceptual correlates of these variables are usually referred to in vision science as *visual features*—simple, rapidly-determined properties that support operations such as grouping texture perception, and attentional selection (Wolfe & Horowitz, 2004; Wolfe & Utochkin, 2019).

But whereas vision science has extensively studied the first three uses of visual variables, it has given relatively little attention to the fourth, viz., the use of visual features to convey quantitative information. Perceived orientation, say, can facilitate such things as grouping and attentional selection, and various models have been proposed as to how this might be carried out (see Wolfe et al., 2002). But how is orientation able to explicitly convey abstract numerical information, as is often done in visualization dashboards and other displays (e.g., Harris, 1999)? What might be the mechanisms involved?

The perception of quantity has, of course, long been studied in the context of perceived sensory magnitude. Starting with the work of Fechner in the 19th century (see e.g., Ross, 1997), this

[1] Technically, there is a fifth: conveying order in a series. For most purposes, however, order can be considered a coarse version of quantity: ordinal values can always be conveyed whenever numerical values can be (Roth, 2017).

eventually developed into the study of sensory scaling (e.g., Billock & Tsou, 2011; Stevens, 1966). A related approach, based on information-theoretic considerations, examined the number of distinct levels or categories of perceived magnitude, yielding the capacity—essentially the signal-to-noise ratio—for the perceptual channels corresponding to various properties (Miller, 1956; Nizami, 2010). But while valuable, such investigations generally focused on the perception of a single sensory property; the quantities involved were usually taken as linked with their sensory qualities in some way (as suggested by conscious experience), with abstraction into pure number occurring at a higher, cognitive level.[2] It has been found that abstract quantity—viz., the number of items in a set—can be perceived within half a second (Burr & Ross, 2008; Cheyette & Piantadosi, 2020). But the relevant quantity here is an integer rather than a continuous number. Moreover, the quantities investigated are the outputs of processes rather than inputs, so that little can be said about the extent to which abstract information might already be available to low-level processes operating in parallel across space.

The goal of this paper, then, is to investigate the extent to which continuous (or at least, non-integer) quantitative information can be carried by visual features, and in particular, the extent to which it can be represented in an abstract form, one not tied to any sensory quality. Towards this end, it is useful to consider perception not *within* perceptual dimensions, but *between* them—in particular, to consider the perception of the Pearson correlation *r* between information conveyed by two different properties. If quantitative information can be combined to support the perception of correlation, it would imply a common form in which the representation of this information has

[2] Similarly, ensemble processes that rapidly estimate the mean value of some property of set of items (Alvarez, 2011; Whitney & Leib, 2018) are also generally examined using j one property at a time.

been separated from the representation of the original sensory properties, allowing it to be combined in the dense fashion typical of low levels of visual processing,

Approach

To see how an approach of this kind might be implemented, consider first the *scatterplot*, a graphical representation where each ordered pair of a dataset is mapped to a dot, with the value of the first data dimension encoded by its horizontal position, and the second its vertical position (Figure 1a). In such a representation, Pearson correlation *r* can be assessed by combining information about the horizontal and vertical position of each dot. Both properties used in this representation are the same (viz., position), and so the information they carry can be combined in a straightforward way.

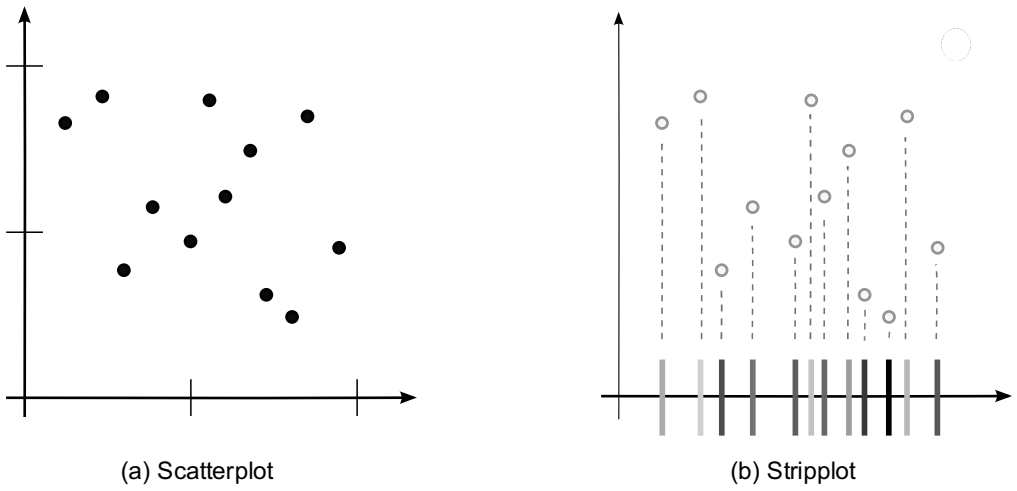

Figure 1. Bivariate stripplot representation. (a) Standard scatterplot. Here, horizontal position represents the value of the first data dimension, and vertical position the second. (b) Bivariate stripplot (position-luminance). Here, horizontal position represents the value of the first data dimension and luminance the second. (Dots in gray show equivalent representation as a scatterplot.)

Consider now a *bivariate stripplot* of the type shown in Figure 1b. Here, the first dimension of each data element is again represented by horizontal position, but the second is now represented

by the value of some other property of the corresponding graphical element (in this case, the luminance of the line segment). To perceive correlation, it is necessary to use the joint values carried by the two features, which must then require a common amodal substrate in which the information from different dimensions can be combined on an item-by-item basis. The issue of whether quantitative information carried by luminance can be combined with that carried by position then takes the form of whether correlation can be perceived in such a stripplot, and if so, whether performance matches—despite the differences in appearance—that for scatterplots.

Perception of Correlation in Scatterplots

For scatterplots, the estimation of correlation—at least when done casually—is largely perceptual, being relatively rapid and much the same for most observers, regardless of their level of statistical training (Doherty, Anderson, Angott, & Klopfer, 2007; Lane, Anderson, & Kellam, 1985; Meyer & Shinar, 1992). Discrimination of perceived correlation—characterized by just noticeable difference (JND)—can be described by (Rensink & Baldridge, 2010; Rensink, 2017)

$$JND(r) = k\,(1/\,b_{\text{disc}} - r) \qquad (1)$$

where *variability* k and *discrimination bias* b_{disc} are such that $0 < k$, $b_{\text{disc}} < 1$. Multiplying both sides by b_{disc} and setting $u = 1 - b_{\text{disc}}r$, this becomes $JND(u) = ku$, an instance of Weber's Law (see Ross, 1997). Meanwhile, the magnitude of perceived correlation $g(r)$ can be described by

$$g(r) = \ln(1 - b_{\text{est}}\,r) \,/\, \ln(1 - b_{\text{est}}) \qquad (2)$$

where *estimation bias* b_{est} is such that $0 < b_{\text{est}} < 1$; again setting $u = 1 - b_{\text{est}}r$, this becomes $g(u) = \ln(u) \,/\, (\ln(1 - b_{\text{est}}))$, an instance of Fechner's Law. For a scatterplot, the values of b_{disc} and b_{est} do not reliably differ from each other, indicating a bias b common to both equations (Figure 2).

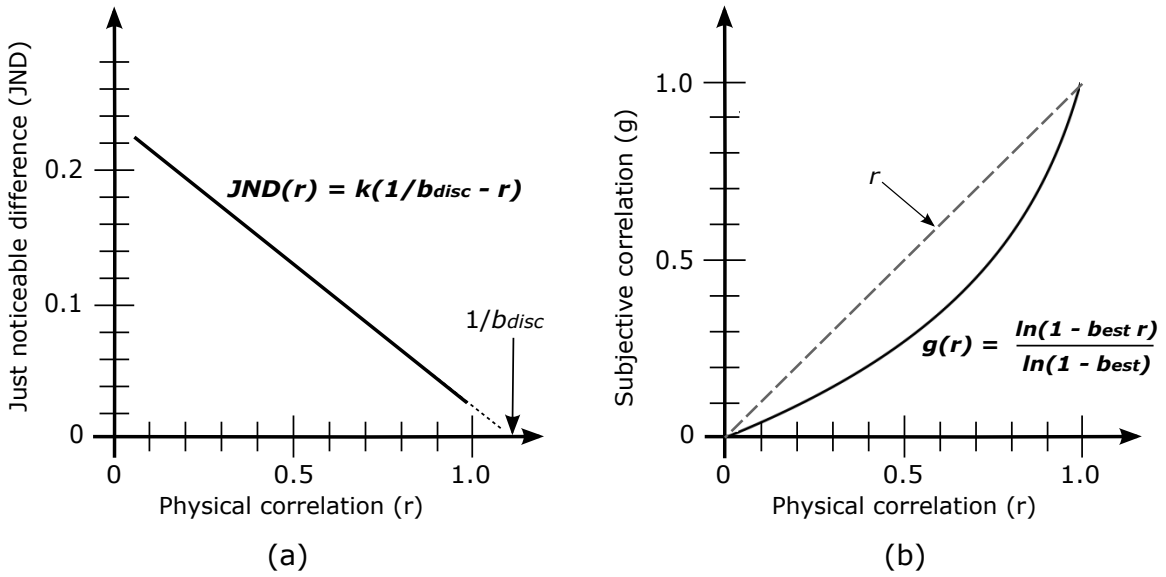

Figure 2. Perception of correlation in scatterplots. (a) Just noticeable difference (JND), via eq. (1). JND decreases as r increases, in direct proportion to distance from $r = 1/b_{disc}$. (b) Perceived magnitude $g(r)$, via eq. (2). This increases as r approaches 1, with the amount of "bend" given by b_{est}. Note that $g(r)$ is never greater than r, with the greatest difference between $g(r)$ and r being for $0.4 \leq r \leq 0.6$. For scatterplots, the two curves are linked, with $b_{disc} = b_{est} = b$. In this figure, $k \approx 0.2$ and $b \approx 0.9$, values typical of scatterplots (Rensink, 2017).

In the situation where $b_{\text{disc}} = b_{\text{est}} = b$, the derivative of (eq. 2) can take the form

$$dg/dr = -[1/(\ln(1-b)] \,/\, [1/b-r].$$

Approximating dr and dg by their finite equivalents Δr and Δg, and rearranging terms,

$$\Delta r = -\Delta g \ln(1-b)\, [1/b - r]. \qquad (3)$$

Assuming that Δg is some *threshold constant* $T_C > 0$ for each Δr = JND (i.e., the Fechner assumption), and matching eq. (3) to eq. (1), it follows that eq. (1) is connected to eq. (2), with

$$k = -T_C \ln(1-b). \qquad (4)$$

Although the physical correlation *r* of a scatterplot is defined via the values of individual horizontal and vertical positions, perceived correlation is not based on the multiplication of these quantities. Instead, it appears to be based on a perceptual proxy: the shape of the probability density function *f (x,y)* that describes the number of elements likely to be encountered at each two-dimensional location in the image; in essence, multiplication is replaced by colocation. More precisely, *entropy theory* (Rensink, 2017) asserts that perceived correlation *g(r)* is proportional to the entropy of the density function *f (x,y)*, where entropy is a measure of disorder (or dispersion) that is proportional to average Shannon information (Ben-Naim, 2008; Stone, 2015). As shown in Appendix A, the entropy for a gaussian distribution is approximately proportional to the logarithm of the width of an *isofraction ellipse,* the set of points at a fixed fraction of the height of *f* (Figure 3). Given the characterization of *g(r)* as entropy, the Fechner assumption of a constant Δg for each Δr takes the form of a constant number of bits for each JND.

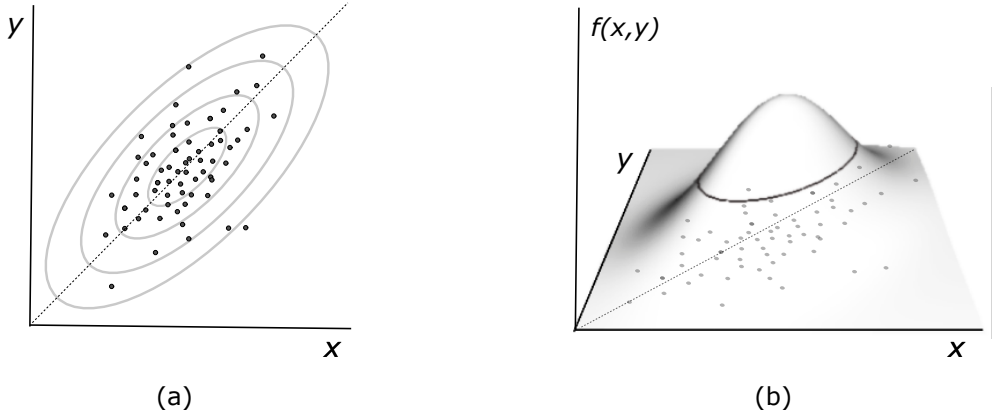

Figure 3. Probability density function f(x,y) for scatterplot dot cloud. (a) Two-dimensional view of a scatterplot with several isopleths (iso-probability contours). (b) Density function *f(x,y*), inferred from the set of dots, showing an isofraction ellipse. Perceived correlation entropy is proportional to the entropy of *f(x,y)*, which is approximately the logarithm of the width of an isofraction ellipse. (Based on Rensink, 2017).

In what follows, the ability of visual features to convey abstract quantitative information is explored by determining the extent to which the perception of correlation in bivariate stripplots

follows eqs. (1) and (2), and whether the Fechner assumption still applies. To the extent that such behavior holds, the feature involved can be considered an *information carrier*—a property able to convey quantitative information in the same way as perceived position, with this information abstracted in a common space in which the information from both perceptual dimensions can be combined. This possibility is investigated for four commonly-used features: luminance, color, orientation, and size.

General Methods

The design of the experiments here is similar to that of Rensink (2017). Each observer was given a discrimination task and an estimation task based on stripplots of various kinds. For the discrimination task, observers were asked to select which of two above-and-below plots was more correlated; for estimation, a test plot positioned between two reference plots was adjusted until its perceived correlation was halfway between those of the references (Figure 4).

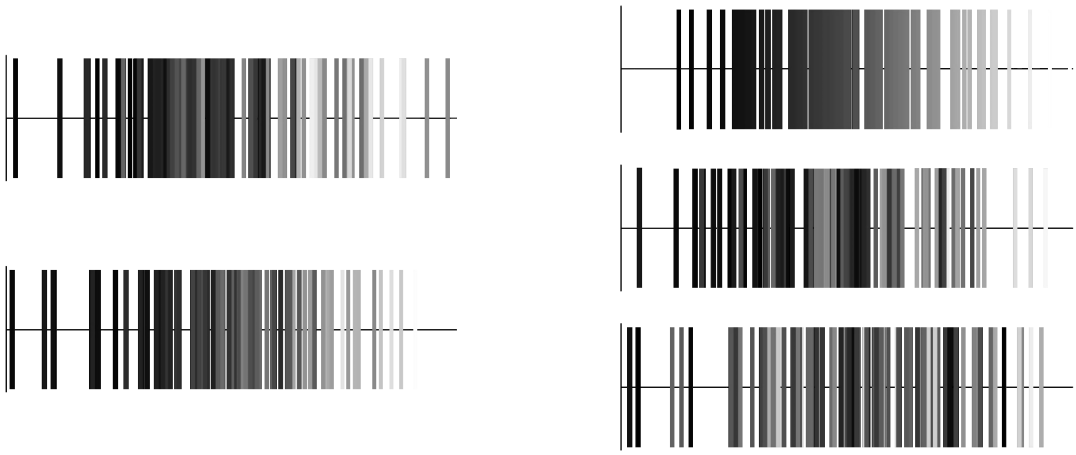

(a) (b)

Figure 4. Schematics of discrimination and estimation tasks. Examples here use stripplots of the type shown in Figure 1. (a) Discrimination. Two above-and-below plots were shown to each observer. Observers were asked to choose the one which appeared more correlated. (b) Estimation. Three stripplots were shown to each observer. Observers adjusted the middle test plot so that its correlation appears to be midway between those of the reference plots at the top (r = 1.0) and bottom (r = 0.0).

All observers carried out both tasks; order was counterbalanced. Observers were told that accuracy was important, but that they could take as much time as needed. To familiarize each observer with the discrimination task, practice trials (with feedback) were given beforehand, starting with $r = 0.0$ and 1.0, and continuing until the observer reached 75% accuracy, or 32 trials had been run. For estimation, 16 practice trials were given; owing to the nature of the task, no feedback could be given for these.

Observers

Each condition had 20 observers, a number chosen to match that used in Rensink (2017). Post-hoc analysis using G*Power (Faul, Erdfelder, Lang, & Buchner, 2007) shows that for this number, an α of 0.05 and effect size d of 0.8 yields power $1-\beta = 0.92$. Different individuals were used in each condition. All were undergraduates at the University of British Columbia, with normal or corrected-to-normal vision; all were paid $10 for a single one-hour session. None had extensive experience with information visualization, although about a quarter had had some exposure to the topic, and almost all had experience with scatterplots. Slightly over half had no formal training in statistics, while most of the remainder had only an introductory course in statistics.

Stimuli

Observers were seated 67 cm from a screen 38.6° × 22.4° in extent, displaying plots that contained gaussian distributions with fixed means and standard deviations. 100 pseudo-random number pairs were generated for each set of data displayed. (For details see Rensink, 2017.) The same dimensions were used for all stimuli. Stripplot axes were 15° wide × 4.2° high, with no tick marks or labels. Stripplot elements (usually line segments) were centered on the horizontal axis, with a

maximum horizontal range of 14.6°. For discrimination, the axes of the stripplots were separated by a vertical distance of 6.8°; for estimation, their separation was 5.0°.

Each dataset had a fixed range of values, with extremes of the numerical range—set here to be 0.0 to 1.0—mapped to the extremes of the range of the visual feature tested. Means were 0.5 of this range, and standard deviations were 0.2, with a straightforward mapping of value to feature. To prevent values from exceeding the bounds of the range [0, 1], any value more than 2.5 standard deviations from the mean was eliminated and a new datapoint generated to take its place.

Procedure - Discrimination

Discrimination was measured via JND, the value Δ for which stripplots containing correlations r and $r \pm \Delta$ can be correctly discriminated about 75% of the time. JND is a measure of percept variability: the greater the JND, the greater the separation needed to see that two plots have different correlations, indicating a greater variability of perceptual estimates; JND is essentially a measure of the "resolution" of the perceptual representation involved.

The procedure to measure JND was that of Rensink (2017). A set of *base correlations* was selected, ranging from 0.0 to 0.9, in steps of 0.1. For each, JND was measured using a series (or *run*) of trials. In each trial, observers were shown two stripplots: one with the base correlation, and the other a test correlation either above or below it (Figure 4). Observers were asked to select the plot that appeared more correlated. If the answer was correct, absolute difference in correlation was decreased by 0.01, making the task more difficult; if incorrect, it was increased by 0.03. (Since 3 steps for each correct answer matched a single step for each incorrect answer, steady-state

performance was approximately 75% correct.) Feedback was provided after each response. New instances were generated every time a response was made, with the relative position of the base and test plots again randomly assigned each time. Performance was assessed via a moving window of 24 consecutive trials, divided into 3 sub-windows of 8 trials each. After 24 trials, average variance within the sub-windows was continually compared to the variance of the sub-window averages (somewhat akin to an *F*-test). Testing halted when this value became sufficiently low (≤ 0.25), or 52 trials had been run; the average of the sub-windows was then taken as the JND.[3] This procedure proved fairly effective, converging for 62% of the runs, and yielding results within 34.9 trials on average.

Order of testing was determined via a latin square design (Kirk, 1995) that counterbalanced base correlations and direction of JND (above vs. below) across the observers; the location of the base correlation stripplot (top vs. bottom) was randomly selected in each trial. To minimize boundary effects (Kay & Heer, 2015), no tests from below were run for base correlations of $r = 0.2$ or less.

Procedure - Estimation

The extent to which an observer can correctly estimate correlation was measured using a bisection technique (Rensink, 2017). Observers were shown two *reference plots* (one with a high level of correlation, one with a low), with a *test plot* in between (Figure 4). The initial value of the test plot alternated between those of the two reference plots, with its correlation adjusted on subsequent presentations until its value appeared to the observer to be halfway between those of the references. All plots (both reference and test) were replaced by new instances every time an adjustment was

[3] For these, the value used was the average of the last 24 trials

made, or 1 second had elapsed[4]. As in the discrimination task, the relative positions of the high and low plots were randomly selected each time to prevent any directional bias, or any accumulation of usable information at the reference locations.

For testing, observers first determined the point subjectively halfway between $r = 0$ and $r = 1$. (These corresponded to $g = 0$ and $g = 1$, respectively). This was done four times, with the mean taken as the physical correlation r corresponding to perceived correlation $g = 1/2$. A second round applied this recursively: observers estimated the point between $g = 0$ and $1/2$ and between $g = 1/2$ and 1; the order of these was counterbalanced. Measurements were again made four times for each subcondition, with averages taken as the values corresponding to $g = 1/4$ and $g = 3/4$. A third round determined the values of r corresponding to subjective estimates $g = 1/8$, $3/8$, $5/8$, and $7/8$; these subconditions were presented in random order.

Analysis

Aggregate results were based on averages of individual responses (see Appendix B). Quantities derived from these (such as k) rarely differed more than a few percent from the averages of derived quantities for individuals, and so are not discussed in detail. JNDs were plotted against adjusted correlation $r_A = r + 0.5\ JND(r)$ when test correlation was from above, and $r_A = r - 0.5\ JND(r)$ when from below. Adjusted correlations are the averages of the base and test correlations; these remove the effects of testing direction (Rensink & Baldridge, 2010). In accord with this, no significant effect of JND direction on derived values was found (all p's > .11); values from both directions

[4] This was to ensure that observers did not unduly weight any particular feature, such as an outlier. It also provided an approximate timing match to discrimination trials, where each display typically appeared for only a second or two.

were therefore pooled. Variability k and bias b_{disc} were obtained via least-squares lines through the resulting set of points. To minimize effects of the boundaries $r = 0$ and $r = 1$ (Kay & Heer, 2015), a *boundary constraint* was imposed: a base correlation was dropped from an experiment if the average ± 1.5 standard deviations fell outside these boundaries for all its conditions. Estimates of b_{est} for individuals were obtained via least-squares fits to their data.[5] Since these estimates generally had high skew, each b value was transformed into the value of r corresponding to $g = ½$; this "midpoint transformation" reduced skew considerably.

Following the recommendations of Cumming (2012), effect sizes are emphasized here: 95% confidence intervals (CIs; shown in square brackets) are provided for all quantities of interest. Unless specified otherwise, comparisons are based on either one-way ANOVAs or two-tailed t-tests. The data and materials for all experiments are available at https://osf.io/2wgb7 (Rensink, 2021a), or upon request. None of the experiments were preregistered.

Experiment 1: Luminance

In this experiment, the value of the first data dimension was encoded by horizontal position and the second by the intensity I of the corresponding graphical element. Intensity is a property often used in information visualization (Roth, 2017); it is also considered a basic visual feature (Turatto & Galfano, 2000). To examine whether intensity (and its perceptual counterpart luminance) supports behavior similar to that for scatterplots, and to examine the extent to which correlation perception is sensitive to the particular mapping used, numerical value v was mapped to intensity

[5] Values for an observer were dropped if the difference between the high and low estimates for the first round of bisections was greater than 0.75 (taken to indicate that the observer did not understand or could not carry out the task). This resulted in 14.5% of observers being dropped, comparable to what was found in studies of scatterplots (e.g., Cleveland, Diaconis, & McGill, 1982; Rensink, 2017).

via $I = v^{\gamma}$ for several different values of γ; these were chosen to be similar to the values used in most video systems (Figure 5). The scaling factor was such that $v = 0.0$ mapped to the minimum luminance of the monitor (1.6 cd/m^2), and $v = 1.0$ to its maximum (52.7 cd/m^2).[6] Values for base correlation $r = 0.3$ from below were dropped due to the boundary constraint.

Observers

Observers in this experiment ranged from 18 to 34 years of age, with an average of 21.9 years. Of the 80 observers for the four conditions (20 in each), 30 were male and 50 were female.

Stimuli

Black backgrounds were used in all conditions in this experiment, with axes and line segments that were white (Figure 5). Line segments were 3.8° long and 0.17° thick. Stimuli for the various conditions are as follows:

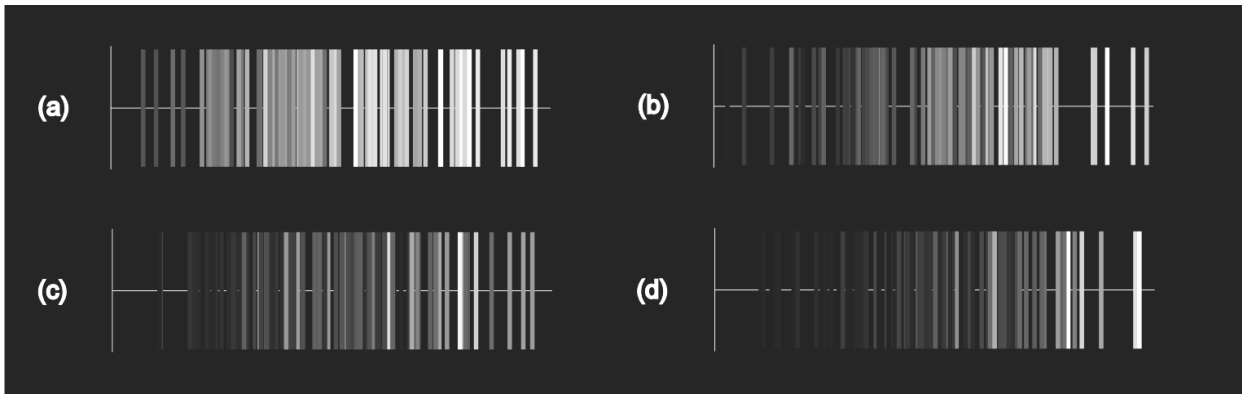

Figure 5. Examples of position-luminance stripplots for various values of γ. For all examples, $r = 0.8$. (a) $\gamma = 1$, corresponding to a direct mapping of value to intensity. (b) $\gamma = 2$, corresponding to common usage in video monitors. (c) $\gamma = 3$, corresponding to the mapping of numerical value to perceived intensity. (d) $\gamma = 4$, a value rarely used due to its extreme nature.

[6] Mappings were created via a lookup table, with γ of the physical device set to 1.0.

Condition 1A: Here, numerical value v was mapped directly to intensity (Figure 5a). This corresponds to the "value" commonly used in information visualization, which is defined as the proportion of energy reflected from a surface, viz., reflectance (Roth, 2017); in a black-and-white display this corresponds to the proportion of white pixels in a given area (Bertin, 1967/2011).

Condition 1B: To create an image that is perceptually clear, most monitors use a γ between 1.8 and 2.2 (Kane & Bertalmio, 2016; Smith, 1995). To test this range of values, this condition used the midpoint of the range, viz., $\gamma = 2$ (Figure 5b).

Condition 1C: Here, $I \propto v^3$ (Figure 5c). Since perceived luminance (or brightness) is roughly proportional to I^{α}, where $\alpha \approx 0.33$ under many conditions (Stevens, 1966), this mapping results in perceived luminance being approximately proportional to numerical value.

Condition D: In this condition, $\gamma = 4$ (Figure 5d), an extreme case that goes beyond the values used in most monitors (Smith, 1995).

Results

Results for condition 1A are shown in Figure 6; as is evident, both discrimination and estimation followed laws similar to those for scatterplots (cf. Figure 2). JND was a reasonably good fit to eq. (1) ($R^2 = .82$; RMSE = 0.028), with variability $k = 0.24$ [0.18, 0.30], not reliably different from the $k = 0.21$ for scatterplots ($p = .335$). However, $b_{disc} = 0.68$ [0.58, 0.75] was considerably lower than the $b_{disc} = 0.90$ encountered there ($p < .001$). Meanwhile, perceived correlation was a good fit to eq. (2) (RMSE = 0.018), with $b_{est} = 0.77$ [0.46, 0.91], a value somewhat less than that of its scatterplot counterplot ($p = .049$).

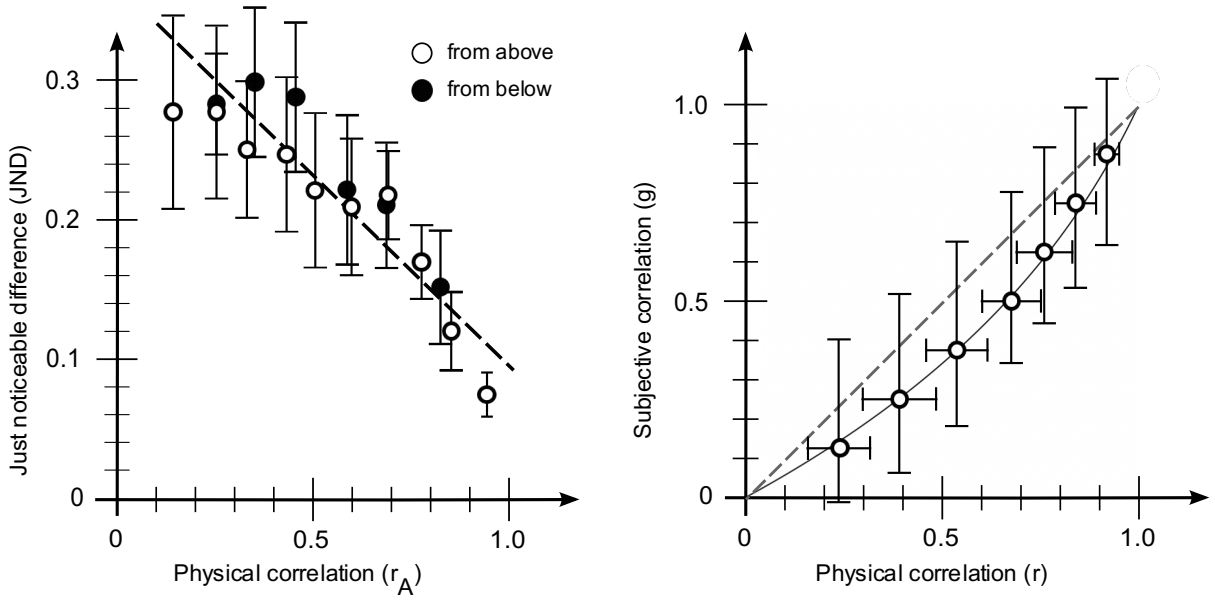

(a) (b)

Figure 6. Results for Condition 1A (γ = 1). (a) Discrimination as measured via JND. Error bars denote 95% CIs. White dots indicate that comparison is against a test correlation from above; black indicate test correlation from below. Best fit of slope to the combined data is $k = 0.25$, and $b_{disc} = 0.69$. (b) Estimation as measured via bisection**.** The curve for perceived correlation is $g(r) = \ln(1 - b_{est} r) / \ln(1 - b_{est})$; best fit is for $b_{est} = 0.77$ Dashed line shows $g(r) = r$ for reference. Horizontal error bars are CIs for estimates of r corresponding to the given values of $g(r)$. Vertical bars show $g(r \pm 1$ JND); the similarity of these lengths indicates the degree to which the Fechner assumption holds.

The key results for Conditions 1A-D are shown in Table 1. (For the aggregate values on which these are based, see Appendix B.) The patterns found in condition 1A clearly extend to the other conditions as well: In all cases, JND was a reasonably linear function of correlation (average $R^2 = 0.86$; RMSE = 0.023), and perceived correlation a logarithmic function (average RMSE = 0.017). Moreover, discrimination and estimation biases did not reliably differ: d_{av} (Cohen's d for paired comparisons) was relatively small (average = 0.22), consistent with the Fechner assumption.

	Discrimination				Estimation		Fechner	
Cond	*k*	R^2	*RSME*	b_{disc}	b_{est}	*RSME*	*p*	d_{av}
S	0.21 *[0.17, 0.25]*	0.97	0.008	0.90 *[0.84, 0.94]*	0.91 *[0.86, 0.95]*	0.018	.686	0.13
1A	0.24 *[0.18, 0.30]*	0.82	0.028	0.68 *[0.58, 0.75]*	0.77 *[0.46, 0.91]*	0.016	.446	0.35
1B	0.21 *[0.15, 0.27]*	0.88	0.020	0.69 *[0.60, 0.77]*	0.72 *[0.43, 0.88]*	0.019	.959	0.02
1C	0.23 *[0.18, 0.27]*	0.88	0.020	0.76 *[0.68, 0.83]*	0.65 *[0.33, 0.83]*	0.017	.236	0.37
1D	0.29 *[0.25, 0.34]*	0.90	0.023	0.84 *[0.74, 0.91]*	0.78 *[0.54, 0.91]*	0.016	.511	0.16
Avg*	**0.23** ***[0.20, 0.25]***	0.86	0.023	**0.71** ***[0.65, 0.77]***		0.017	.972	0.22

Table 1: Main results for Experiment 1 (luminance). Fechner: If the Fechner assumption holds ($b_{disc} = b_{est}$), the difference between them would be statistically insignificant ($p \gtrsim .05$) and Cohen's *d* small ($d_{av} \lesssim 0.2$). Values for scatterplots (S) from Experiment 1 of Rensink (2017). * = Average for conditions 1A-1C. Average R^2, *RSME,* and d_{av} are direct averages; values for *k*, *b*, and *p* from pooled data.

Analysis of combined results fails to show a reliable tendency for γ to affect *k* ($F(3,76) = 1.858$; $p = .144$), although it did have a clear effect on b_{disc} ($F(3,76) = 3.907$; $p = .012$). For $1 \leq \gamma \leq 3$, no dependence on γ was evident for *k* ($F(2,57) = 0.235$; $p = .791$) or b_{disc} ($F(2,57) = 1.445$; $p = .244$). For $\gamma = 4$, *k* was significantly higher than for the other conditions ($k = 0.29$ [0.25, 0.34]; $p = .026$), as was discrimination bias ($b_{disc} = 0.84$ [0.74, 0.91]; $p = .003$). No significant effect of γ on b_{est} was evident ($F(3,56) = 0.379$; $p = .768$).

Discussion

In spite of their different appearance, position-luminance stripplots give rise to behavior strikingly similar to that for scatterplots: precision and accuracy are described reasonably well by linear and logarithmic laws respectively, and discrimination and estimation biases did not markedly differ, in line with the Fechner assumption. Luminance therefore appears to be an information carrier, with performance much the same for $1 \leq \gamma \leq 3$. For $\gamma = 4$, the higher JNDs (reflected in greater k and b_{disc}) may arise from the distortions created by this extreme mapping; such distortions, however, do not appear to significantly affect perception of correlation magnitude.

Experiment 2 – Color

The next feature examined was color. Color differs from luminance in that it varies in quality (hue) rather than quantity (intensity). Nevertheless, color is widely used in information visualization (Roth, 2017) as well as being a well-known visual feature (Turatto & Galfano, 2000; Wolfe & Horowitz, 2004). Given the results for luminance, it might then be expected that similar performance would be encountered. To test this, three mappings were examined: two based on approximations of the basic "opponent" dimensions believed to exist for color (Ware, 2012), and the third a rainbow map, a popular design that maps values to the wavelength of the colors, which involve multiple color dimensions (Reda & Szafir, 2021). Values for all base correlations were consistent with the boundary constraint.

Observers

Ages ranged from 18 to 35, with an average of 21.3 years. Only observers who reported themselves as color-normal were used. Of the 60 observers (20 in each condition), 18 were male and 42 female.

Stimuli

Stimuli here were much like those in Experiment 1, except with numerical values mapped to positions on a color continuum rather than intensity (Figure 7). White backgrounds were used in all conditions, with black axes. Lines were vertical segments 3.8° long and 0.17° wide, so that apart from their color, the graphical representations were similar to those used for luminance. Stimuli for the individual conditions are as follows:

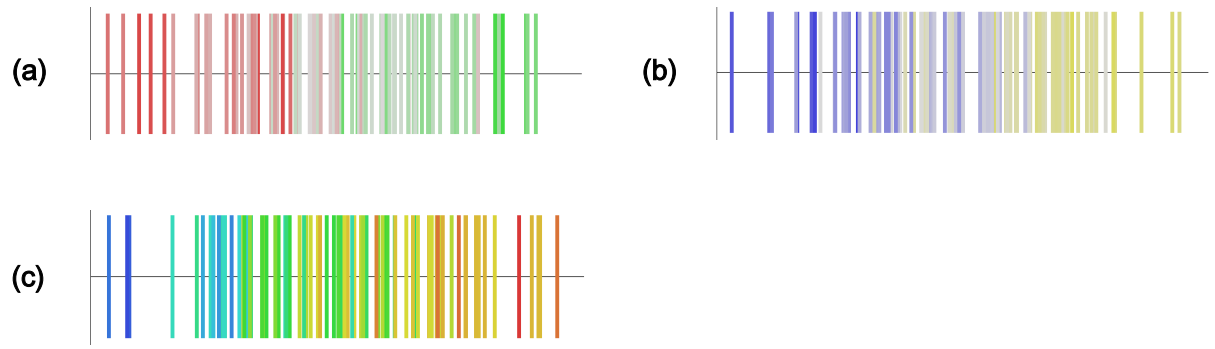

Figure 7. Examples of position-color stripplots for various color maps. For all examples, $r = 0.8$. (a) Red-green, loosely corresponding to one of the two color dimensions in human perception. (b) Blue-yellow, loosely corresponding to the second color dimensions. (c) Rainbow map, a common design used in information visualization, in which colors are arranged according to wavelength.

Condition 2A: Numerical value was mapped to a red-green continuum formed by linearly interpolating endpoint colors red (L*a*b* = 60.1, 47.8, 28.0) and green (L*a*b* = 77.7, -44.9, 50.4), with these being approximately isoluminant.

Condition 2B: The same as condition 2A, except the endpoints of the continuum were blue (L*a*b* = 49.1, 33.7, -87.1) and yellow (L*a*b* = 84.7, -13.3, 74.7). Together with the red-green continuum of Condition 2A, these colors roughly approximate the two opponent color dimensions believed to exist in human vision (Buchsbaum & Gottschalk, 1983; Ware, 2012).

Condition 2C: This used a rainbow map, a popular scheme in which colors are mapped to physical wavelength; in contrast to the previous two color conditions, this does not correspond to a well-defined perceptual dimension. Although such a mapping often leads to poor performance, possibly due to the grouping of distant numerical values represented by colors that are perceptually close, rainbow maps are still commonly used in visualization (Borland & Taylor, 2007; Reda & Szafir, 2021; Ware, 1988).

Results

Results for condition 2A are shown in Figure 8. JND was again a good fit to eq. (1) (R^2 = .87; RMSE = 0.016). Variability k = 0.17 [0.12, 0.21] was not found to differ significantly from that for scatterplots (p = .144), while b_{disc} = 0.67 [0.57, 0.75] was considerably lower (p < .001). Perceived correlation also fit eq. (2) reasonably well: RMSE = 0.041. Bias b_{est} = 0.60 [0.22, 0.80] was also significantly lower than its scatterplot counterpart (p = .001). Its value did not differ significantly from b_{disc} (p = .568).

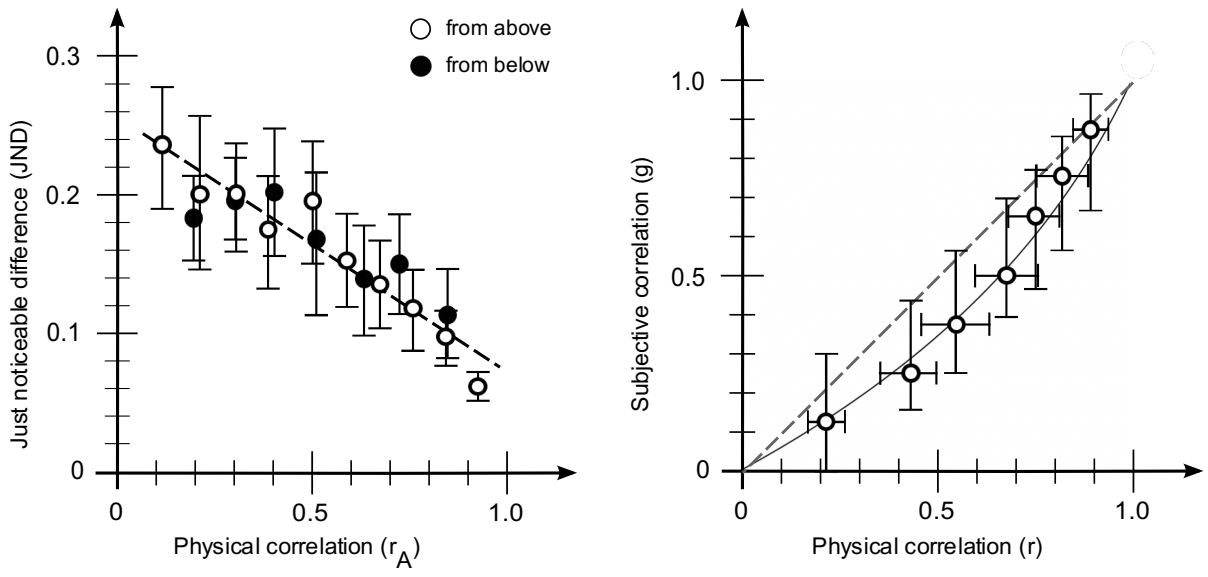

(a) (b)

Figure 8. Results for Condition 2A (color; isoluminant red-green). (a) Discrimination as measured via JND. Error bars denote 95% CIs. White dots indicate that comparison is made against a test correlation from above; black indicate test correlation from below. Best fit of slope to the combined data is $k = 0.17$, and $b_{disc} = 0.68$. (b) Estimation as measured via bisection**.** The curve for perceived correlation is $g(r) = \ln(1 - b_{est}\, r) / \ln(1 - b_{est})$; best fit is for $b_{est} = 0.74$ Dashed line shows $g(r) = r$ for reference. Horizontal error bars are CIs for estimates of r corresponding to the given values of $g(r)$. Vertical bars show $g(r \pm 1$ JND); similarity indicates the degree to which the Fechner assumption holds.

The main results for all conditions are shown in Table 2 (see Appendix B for aggregate values). In general, JND was a clear linear function of r (average $R^2 = 0.86$ and RMSE = 0.016), and perceived correlation a logarithmic function (average RMSE = 0.037). No significant differences were found between the two axes (k: $p = .448$; b_{disc}: $p = .545$; b_{est}: $p = .972$), nor were significant differences found between b_{disc} and b_{est} for either axis ($p > .5$ for both). The rainbow map, however, differed reliably from these in k and b_{disc} (both p's < .001), although not b_{est} ($p = .838$). In contrast to earlier conditions, a significant difference was now found between b_{disc} and b_{est} ($p = .038$; $d_{av} = 0.70$),

suggesting that the Fechner assumption did not hold in this condition. No significant overall effect of condition was found for b_{est} ($F(2,50) = 0.021$; $p = .979$).

	Discrimination				Estimation		Fechner	
Cond	*k*	R^2	*RSME*	b_{disc}	b_{est}	*RSME*	*p*	d_{av}
S	0.21 *[0.17, 0.25]*	0.97	0.008	0.90 *[0.84, 0.94]*	0.91 *[0.86, 0.95]*	0.018	.686	0.13
2A	0.17 *[0.12, 0.21]*	0.87	0.016	0.67 *[0.57, 0.75]*	0.60 *[0.22, 0.80]*	0.041	.563	0.20
2B	0.14 *[0.11, 0.18]*	0.85	0.016	0.63 *[0.52, 0.72]*	0.60 *[0.17, 0.82]*	0.032	.746	0.11
2C	0.27 *[0.23, 0.32]*	0.93	0.013	0.85 *[0.77, 0.90]*	0.63 *[0.25, 0.83]*	0.016	**.038**	**0.70**
Avg*	**0.15** ***[0.13, 0.18]***	0.86	0.016	**0.63** ***[0.52, 0.71]***		0.037	.556	0.15

Table 2: Main results for Experiment 2 (color). Fechner: If the Fechner assumption holds ($b_{disc} = b_{est}$), the difference between them would be statistically insignificant ($p \gtrsim .05$) and Cohen's *d* small ($d_{av} \lesssim 0.2$). Values for scatterplots (S) from Experiment 1 of Rensink (2017). * = Average for conditions 2A and 2B. Average R^2, *RSME,* and d_{av} are direct averages; values for *k*, *b*, and *p* from pooled data.

Discussion

Each color axis supported behavior much like those for luminance and position, pointing to all three being information carriers. In addition, the two opponent-color axes give rise to performance similar to each other in all regards, suggesting that they convey information in much the same way. The JNDs for the rainbow mapping are much higher than for the other two conditions and do not obey the Fechner assumption, suggesting that some additional factor may be at play when stimuli do not correspond to single perceptual dimension.

Experiment 3: Orientation

The next set of conditions examined the representation of quantity by orientation. As for the case of color, orientation encodes values via location along a finite continuum; however, orientation is a geometric rather than a radiometric property. Orientation is often used in information visualization to convey quantitative information (Roth, 2017) and is also a basic visual feature (Wolfe & Horowitz, 2004). Given these considerations (and the results of the previous experiment), it may be expected that results here will resemble those for position, luminance, and color. Because orientation requires a line, and the length of the lines could impact performance, three different mappings were examined: (a) constant length of lines, (b) random length of lines, and (3) constant height of the outline of the set of lines (Figure 9). For all of these, orientations ranged from -45° to 45°, with mean quantitative value (0.5) mapped to vertical. Values for base correlations $r = 0.3$ and $r = 0.4$ from below were dropped due to the boundary constraint.

Observers

Ages ranged from 18 to 33, with an average of 22.3 years. Of the 60 observers (20 in each condition), 24 were male and 36 female.

Stimuli

All conditions used white backgrounds, with axes and line segments that were black. Line segments were 1 pixel (0.02°) wide, resulting in graphical representations of the form shown in Figure 9. The particular stimuli for the various conditions are as follows:

Condition 3A: Line lengths were set to 4.0°. Although this controlled for line length, the resulting line arrays had outlines that could potentially give information about *r* (Figure 9a).

Condition 3B: To determine if the outlines of the arrays influence performance, line lengths were randomly varied between 0.8° and 4.0° (uniform distribution); this resulted in representations where outlines are no longer distinct (Figure 9b).

Condition 3C: As an alternate way of reducing the possible effect of the outlines, the lengths of lines were adjusted to that the outline had a fixed height of 4.0°, and so unable to contain any information about correlation (Figure 9c).

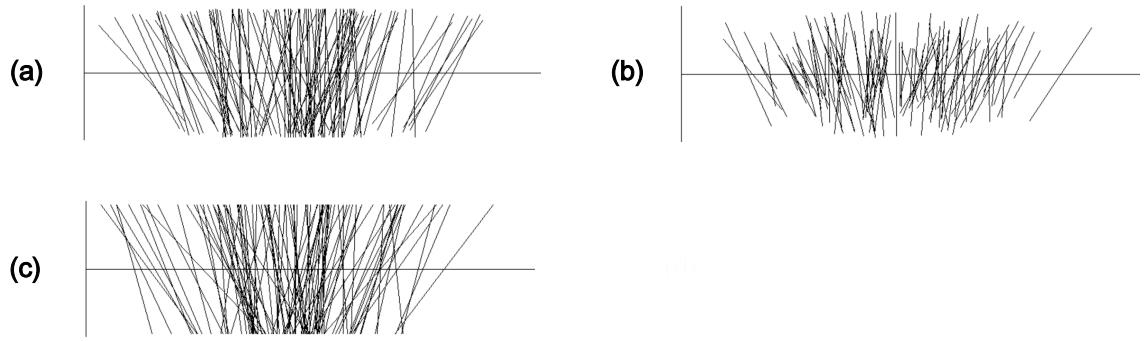

Figure 9. Examples of position-orientation stripplots. For all examples, $r = 0.8$. (a) Fixed length of lines. (b) Random length of lines. (c) Fixed height of outline.

Results

Performance for condition 3A is shown in Figure 10. JND was again a good fit to eq. (1) ($R^2 = .91$; RMSE = 0.030). Variability $k = 0.39$ [0.30, 0.49] was significantly higher than its counterpart for scatterplots ($p < .001$), but not so for $b_{disc} = 0.90$ [0.80, 0.96] ($p = .951$), and $b_{est} = 0.92$ [0.82, 0.97] ($p = .772$). Perceived correlation was again a reasonably good fit to eq. (2): RMSE = 0.029, with b_{est} not significantly different from b_{disc} ($p = .725$).

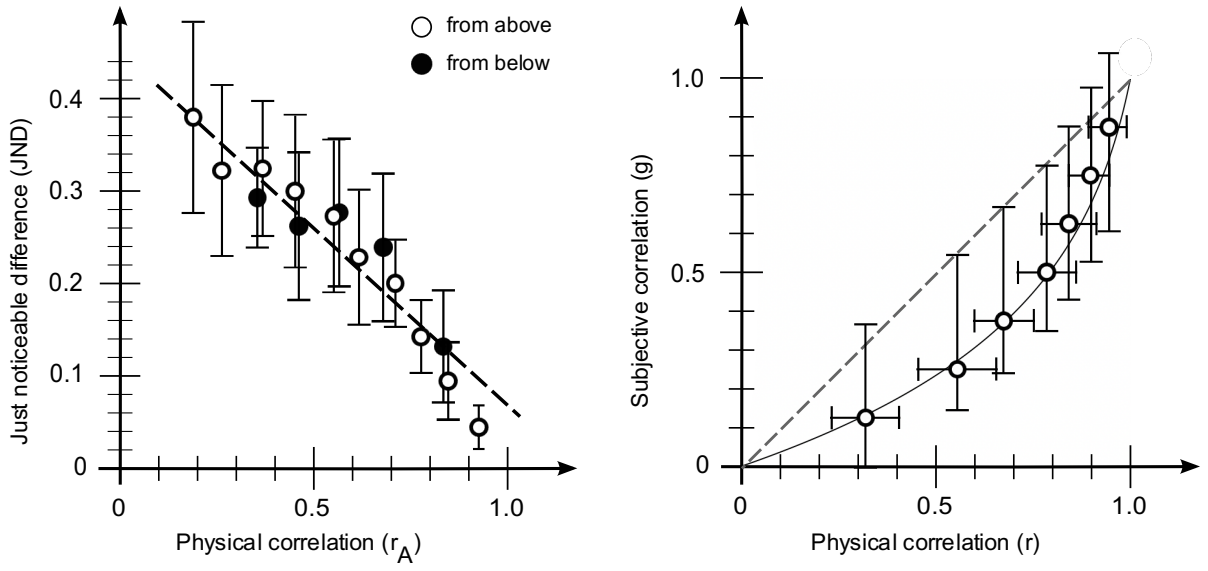

(a) (b)

Figure 10. Results for Condition 3A (orientation; fixed length). (a) Discrimination as measured via JND. Error bars denote 95% CIs. White dots indicate that comparison is made against a test correlation from above; black indicate test correlation from below. Best fit of slope is $k = 0.40$, and $b_{disc} = 0.87$. (b) Estimation as measured via bisection**.** The curve for perceived correlation is $g(r) = \ln(1 - b_{est} r) / \ln(1 - b_{est})$; best fit is for $b_{est} = 0.94$. Dashed line shows $g(r) = r$ for reference. Horizontal error bars are CIs for estimates of r corresponding to the given values of $g(r)$. Vertical bars show $g(r \pm 1$ JND); their similarity in length indicates the degree to which the Fechner assumption holds.

The main results for all conditions are presented in Table 3. (For aggregate values, see Appendix B.) In all cases, JND was a clear linear function (average $R^2 = 0.92$; RMSE = 0.027), and perceived correlation a logarithmic function (average RMSE = 0.020). No reliable effect of condition was found on variability k ($F(2,57) = 1.362$; $p = .264$), b_{disc} ($F(2,57) = 0.121$; $p = .886$), or b_{est} ($F(2,52) = 0.019$; $p = .981$). And as in the case of position, luminance, and color, no reliable difference was found between b_{disc} and b_{est} in general ($p = .234$), nor was d_{av} very large (= 0.17), consistent with the Fechner assumption.

	Discrimination				Estimation		Fechner	
Cond	k	R^2	*RSME*	b_{disc}	b_{est}	*RSME*	p	d_{av}
S	0.21 *[0.17, 0.25]*	0.97	0.008	0.90 *[0.84, 0.94]*	0.91 *[0.86, 0.95]*	0.018	.686	0.13
3A	0.39 *[0.30, 0.49]*	0.91	0.030	0.90 *[0.80, 0.96]*	0.92 *[0.82, 0.97]*	0.029	.725	0.10
3B	0.38 *[0.32, 0.44]*	0.95	0.027	0.90 *[0.83, 0.95]*	0.92 [*0.87, 0.96]*	0.019	.648	0.15
3C	0.32 *[0.25, 0.38]*	0.90	0.025	0.88 *[0.77, 0.95]*	0.93 *[0.87, 0.97]*	0.012	.460	0.26
Avg	**0.36 *[0.32, 0.40]***	0.92	0.027	**0.91 *[0.88, 0.94]***		0.020	.234	0.17

Table 3: Main results for Experiment 3 (orientation). Fechner: If the Fechner assumption holds ($b_{disc} = b_{est}$), the difference between them would be statistically insignificant ($p \gtrsim .05$) and Cohen's d small ($d_{av} \lesssim 0.2$). Values for scatterplots (S) from Experiment 1 of Rensink (2017). Averages for all conditions. Average R^2, *RSME,* and d_{av} are direct averages; values for k, b, and p from pooled data.

Discussion

Once again, performance followed much the same laws as those for the other features. Performance was much the same for all conditions, indicating that neither the outlines of the stimuli in condition 3A nor the random changes in length in conditions 3B had much effect. As such, these results indicate that orientation was indeed the main factor governing performance, and that—like position and luminance—it is an information carrier.

Experiment 4 – Size

A final experiment examined size. Size differs from the other features examined here in that it is *extensive*—i.e., given the right conditions, values assigned to adjoining components in the image can be added together (see e.g., Carnap, 1966). Nevertheless, size is often used to convey

quantitative information (Roth, 2017) and is also considered a basic visual feature (Wolfe & Horowitz, 2004). Consequently, it might still be expected that performance would be similar to that for the other features examined here. Note that an ambiguity exists when referring to 'size', since this could mean either length or area. To be clear, then, values here were mapped to the length of one-dimensional lines, as well as to the diameter of two-dimensional circles, with lengths and diameters varying between 0.08° – 4.0°. Values for base correlation $r = 0.3$ from below were dropped due to the boundary constraint.

Observers

Ages ranged from 18 to 26, with an average of 20.4 years. Of the 40 observers for the two conditions (20 in each), 5 were male and 35 female.

Stimuli

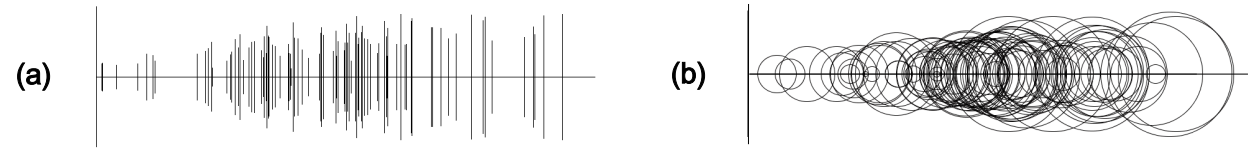

Figure 11. Examples of position-size stripplots. For all examples, $r = 0.8$. (a) Vertical lines varying length. (b) Circles of varying diameter.

White backgrounds were again used, with axes and lines that were black and 1 pixel (0.02°) wide.

Condition 4A: This examined the direct mapping of value v to length, with the graphical elements being thin vertical lines (Figure 11a).

Condition 4B: This used stripplots where value v was mapped to the diameter of a circle (Figure 11b). Diameters had the same range of sizes as the lengths in condition A.

Results

Results for condition 4A are shown in Figure 12. JND was again a good fit to eq. (1) (R^2 = .91; RMSE = 0.020), with variability k = 0.26 [0.21, 0.31] and bias b_{disc} = 0.83 [0.76, 0.89]. Perceived correlation was also a good fit to eq. (2): RMSE = 0.010, and b_{est} = 0.73 [0.50, 0.86], a value not significantly different from b_{disc} (p = .133).

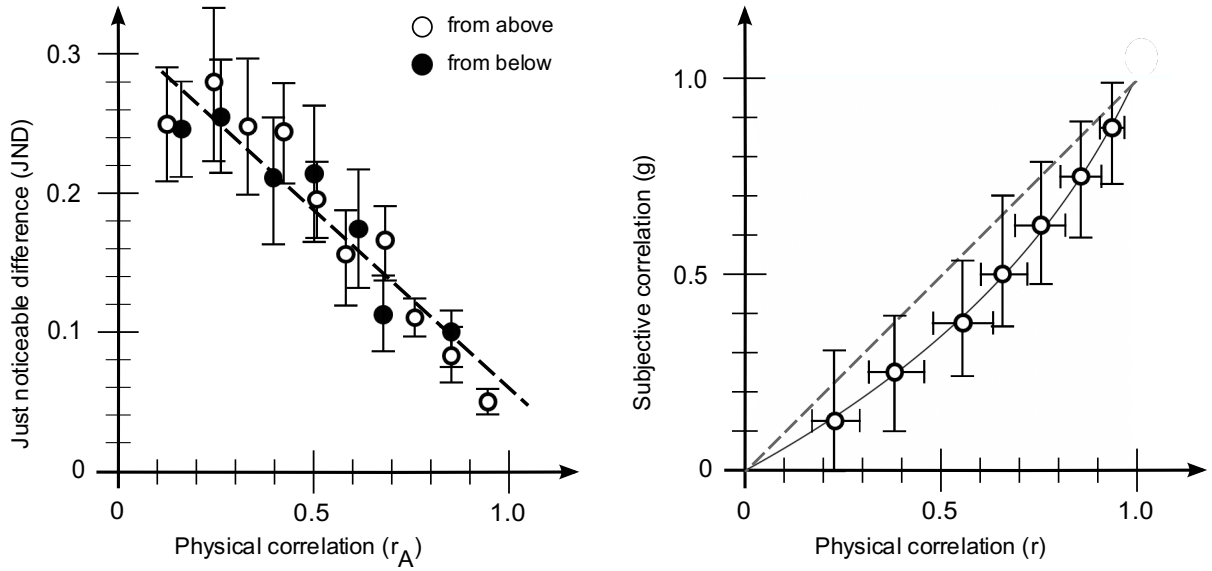

(a) (b)

Figure 12. Results for Condition 4A (size; line length). (a) Discrimination as measured via JND. Error bars denote 95% CIs. White dots indicate that comparison is made against a test correlation from above; black indicate test correlation from below. Best fit of slope to the combined data is k = 0.28, and b_{disc} = 0.85. (b) Estimation as measured via bisection**.** The curve for perceived correlation is $g(r) = ln(1 - b_{est}\, r) / \ln(1 - b_{est})$; best fit is for b_{est} = 0.73. Dashed line shows $g(r) = r$ for reference. Horizontal error bars are CIs for estimates of r corresponding to the given values of $g(r)$. Vertical bars show $g(r \pm 1$ JND); their similarity indicates the degree to which the Fechner assumption holds.

Main results for both conditions are shown in Table 4. (Underlying aggregate values are given in Appendix B.) In all cases, JND was again alinear function of r (average R^2 = 0.92 and RMSE = 0.019), and perceived correlation a good fit to the logarithmic function (average RMSE = 0.021). No reliable difference was found between the two in variability k (p = .907) or discrimination bias

b_{disc} (p = .747). While no significant difference was found between b_{disc} and b_{est} for the lines (p = .13), a much larger and more reliable difference was found for the circles, with b_{est} significantly higher than b_{disc} (p = .029), and d_{av} approaching a value of 1.

	Discrimination				Estimation		Fechner	
Cond	k	R^2	*RSME*	b_{disc}	b_{est}	*RSME*	p	d_{av}
S	0.21 *[0.17, 0.25]*	0.97	0.008	0.90 *[0.84, 0.94]*	0.91 *[0.86, 0.95]*	0.018	.686	0.13
4A	0.26 *[0.21, 0.31]*	0.92	0.020	0.83 *[0.76, 0.89]*	0.73 *[0.50, 0.86]*	0.010	.130	0.50
4B	0.25 *[0.20, 0.31]*	0.92	0.018	0.82 *[0.73, 0.88]*	0.93 *[0.88, 0.96]*	0.031	**.029**	**0.89**
Avg	**0.26 *[0.22, 0.29]***	0.92	0.019	**0.83 *[0.77, 0.87]***	—	0.021	—	—

Table 4: Main results for Experiment 4 (size). Fechner: If the Fechner assumption holds (b_{disc} = b_{est}), the difference between them would be statistically insignificant ($p \gtrsim .05$) and Cohen's d small ($d_{av} \lesssim 0.2$). Values for scatterplots (S) from Experiment 1 of Rensink (2017). Averages do not include b_{est} (and related measures), since that value differs significantly from b_{disc}. Average R^2, *RSME,* and d_{av} are direct averages; values for k, b, and p from pooled data.

Discussion

For the most part, behavior followed the same laws as for other features, the only exception being that for circles, b_{est} was markedly higher than b_{disc}. The similarity may have been due to the relevant property for circles involving separate width and height estimates (Morgan, 2005), with the result treated as something like length (Raidvee, Toom, Averik, & Allik, 2020); the inequality may have been due to the greater overlap in the circles creating additional noise in discrimination, and so lowering b_{disc} relative to b_{est}.

General Discussion

The experiments here show that visual features can support the perception of correlation, and that despite the strikingly different appearances of the stimuli involved, behavior for all features is largely the same (and the same as for scatterplots). In particular, discrimination follows the Weber-like law described by eq (1), while perceived magnitude follows the Fechner-like law described by eq. (2). (The Weber-like law for discrimination also seems to hold for several other visualization designs (Harrison, Yang, Franconeri, & Chang, 2014).) And for the case of single visual features, the two equations are connected via the Fechner assumption, with no significant difference found between discrimination bias b_{disc} and estimation bias b_{est}, which can then be taken to describe a common bias b. It therefore appears that the features of luminance, color, orientation, and size are all carriers, able to convey abstract quantitative information and combine it across different perceptual dimensions in much the same way as spatial position, with performance differing only in the values of parameters k and b (Figure 13). More complex properties also appear to give rise to similar behavior, except that the Fechner assumption no longer holds.

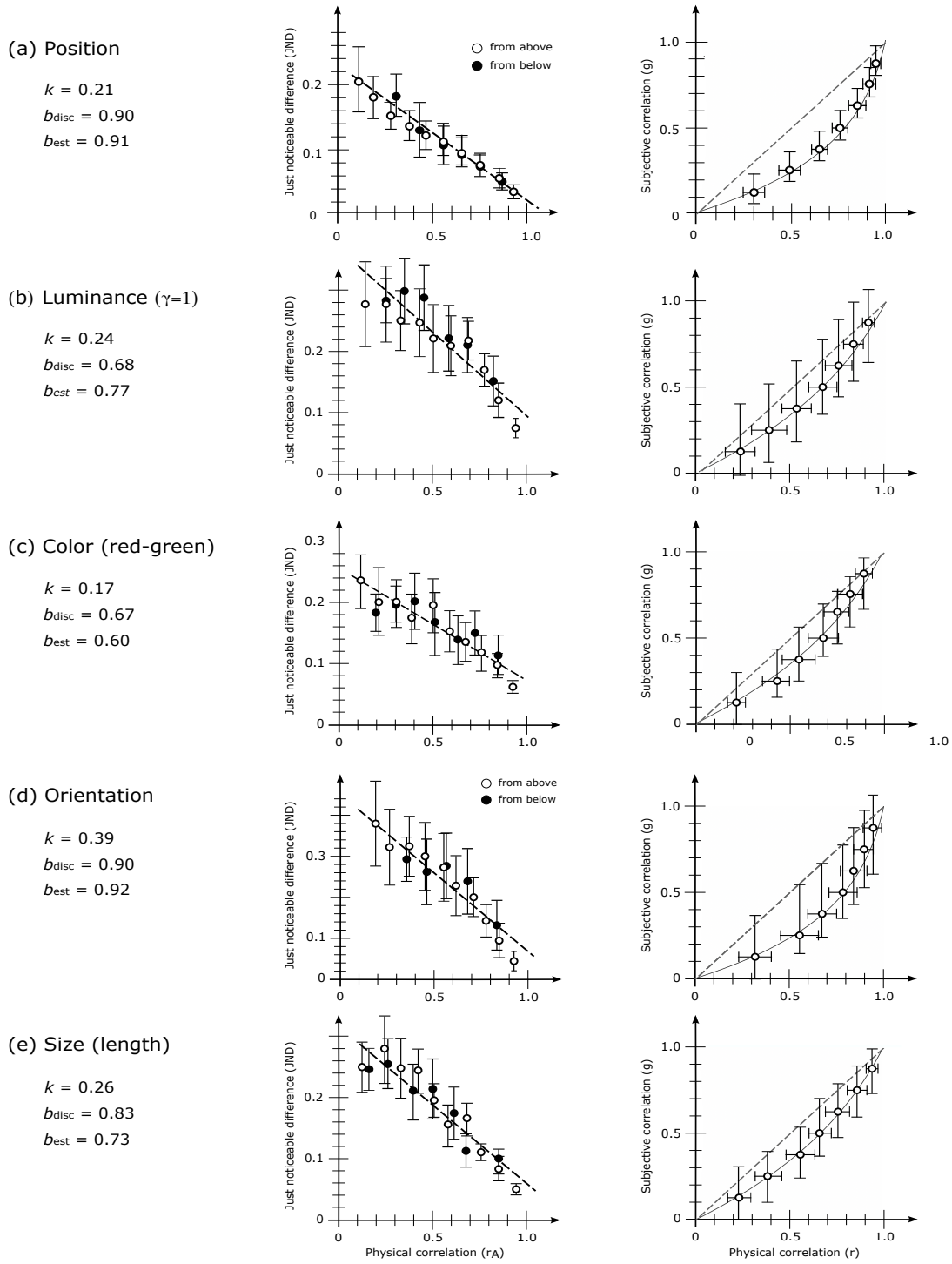

Figure 13. Overview of perception of correlation in various carriers. (a) Position (scatterplots). Data from Rensink (2017). (b) Luminance. Results for condition A ($\gamma = 1$) of Experiment 1. (c) Color. Results for condition A (red-green) of Experiment 2. (d) Orientation. Results for condition A (fixed length) of Experiment 3. (e) Size. Results for condition A (length) of Experiment 4. As is evident, performance for all carriers appears to follow the same general laws, varying only in the parameters k, b_{disc}, and b_{est}, with the latter two not appearing to reliably differ.

Theoretical Implications

To develop the implications of these results, consider first how a visualization system is able to convey quantitative information from a dataset to an observer. This involves a series of stages that essentially form a transmission pipeline, mapping information from a numerical space in the dataset to a perceptual space in the observer (Figure 14). Three perspectives are relevant :

i. the *signal*—the quantitative information conveyed to the observer, viz., the numerical value(s) attached to each item. Ideally, this information remains uncorrupted across all stages of the visualization process, with little noise or distortion introduced during transmission from dataset to perceiver.

ii. the *carrier*—the property that encodes the signal. It has two aspects: the *physical* property that encodes information (e.g., the intensity of a line segment), and the corresponding *perceptual* property in the observer (e.g., its luminance). Note that the encoding conveys quantitative information implicitly—it uses the representation of the carrier property itself (e.g., its intensity).

iii. the *substrate*—the structure that contains the carrier. In the case of a stripplot, for example, this could be a line element, with properties such as luminance, orientation, and position. Again, two aspects can be distinguished: the *physical* structure (e.g., the line segment in the image), and the corresponding *perceptual* representation of that segment.

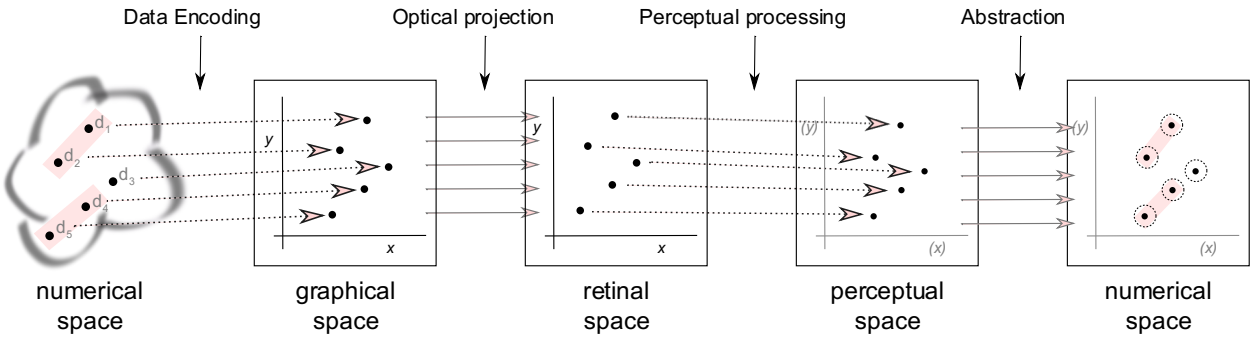

Figure 14. Information visualization pipeline. The transmission of information from one numerical space (that in the dataset) to another (that in the observer) is often viewed as involving three stages: data encoding, optical projection, and perceptual processing, The results here show the need for a fourth stage: an abstraction (or *decoding*) stage, in which the representation of sensory quantities is removed, with representation only of abstract numerical quantity remaining. Ideally, the overall process ensures that equal distances between elements in the numerical space in the dataset (e.g., d_1 to d_2, and d_3 to d_4) map to equal distances in the numerical space in the perceiver (corresponding circles). The effectiveness of the mapping depends on how well encoding / decoding can compensate for the effects of optical and perceptual distortions.

In a scatterplot, for example, the two values of each data element (initially abstract quantities) are encoded by the horizontal and vertical co-ordinates of the corresponding dot on the computer screen; when viewed, the resulting graphical representation yields a low-level perceptual map—e.g., a primal sketch (Marr, 1982)—in which the values in each element are now represented by the two-dimensional location of its corresponding perceptual substrate (i.e., the representation of the corresponding dot). The finding that information from different perceptual dimensions can be combined in a carrier-indifferent form implies that the contents of this perceptual space can be transformed back into abstract form via a decoding process of some kind, resulting in a two-dimensional numerical space with no direct linkage to the properties of the carriers used.

Ideally, the mapping between the numerical spaces in the dataset and in the observer should be *isometric*: equal distances in the original numerical space should map to equal distances in the

numerical space of the observer (Figure 14). To the extent that the decoding process can compensate for the various optical and perceptual effects encountered along the way, distortion will be minimal, and accuracy highest.

What might such a process involve? Among other things, it would likely retain information about the center of mass of each perceptual element (the substrate) along with the value of the relevant carrier (its luminance, say), with all other information likely being discarded. (This might, for example, explain why the variation in length of the segments in the position-orientation stripplots of Experiment 3 had no reliable effect—such information was simply not represented.) And to enable correlation to be perceived, this information must be integrated via an element-by-element binding similar to that of individual horizontal and vertical co-ordinates in a scatterplot. The existence of a dense binding of this form across space suggests that the processes involved are likely carried out at relatively low levels of visual processing, which typically involve a considerable degree of parallel processing (see e.g., Marr, 1982).

Parameter Space Theory

One way to implement abstraction and binding of the kind described above is via *parameter space,* a low-level map in which the representation of sensory qualities is entirely abstract.[7] For a position-luminance stripplot of the type shown in Figure 1, for example, parameter space would be a two-dimensional subspace spanned by the dimensions of horizontal position and luminance value (Figure 15).

[7] Parameter space itself does have a spatial structure in terms of the distances between its elements (hence its name). But the values represented this way are abstract, in that they are not linked to any representation of geometric space or any other sensory quality. Geometric space may be represented directly via a map of some kind, but if so, it is the only such property.

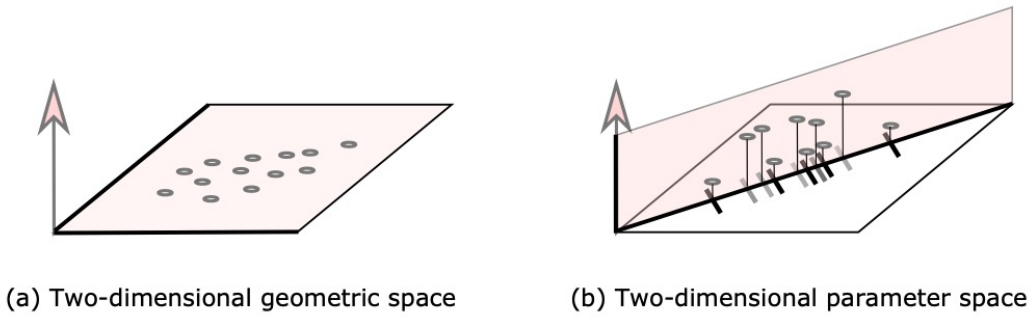

Figure 15. Parameter space. (a) Two-dimensional geometric space formed via two dimensions of spatial position. Values are anchored to position in both dimensions; this is the basis of representations for scatterplots; a probability density function would describe the likelihood of a dot at a particular horizontal and vertical location. (b) Two-dimensional subspace formed via a slice through a three-dimensional parameter space composed of two spatial and one carrier dimension; the probability density function here would describe the likelihood of an element at a particular (one-dimensional) location along the slice, together with a particular luminance value. Values are anchored to position in the spatial dimension, while values in abstract dimensions are normalized to form a gaussian distribution with a fixed mean and variance (taken to be the same in all dimensions).

Two considerations are particularly important in regards to this mapping. The first is the considerable invariance of performance found for variations in most mappings (e.g., different values of γ), which suggests a *normalization* process of some kind. A simple form of this would be a linear rescaling of carrier values to a particular mean and variance; to deal with distortions such as those created by the power functions typical of perceived physical quantities (Ross, 1997), a more sophisticated mapping might be used—e.g., assume a gaussian distribution and take the most common carrier value to be the mean, with other values assigned accordingly. (The increase in JNDs for $\gamma = 4$ and for the rainbow map may reflect the limits of this process.) Such normalization would allow the information carried by sensory magnitude or position to be replaced by dimensionless quantities that are expressed in terms of standard deviations (akin to, say, *z*-scores in statistics). Also important is the relative size of the quantities in different dimensions; if the standard deviations in both dimensions are set to be the same, the resulting *equalization* would

create a common scale between different carriers.[8] The net result of such normalization and equalization would be a data-to-perception mapping that is largely isometric, providing good—and possibly maximal—sensitivity to the statistical structure present (cf. Simoncelli & Olshausen, 2001).

Limited—but interesting—evidence exists for a space of this type. To begin with, representations at early levels of visual processing can describe shape in a manner indifferent to the medium used (e.g., Cavanagh, Arguin, & von Grünau, 1989; Kasai, Morita, & Kumada, 2007), in accord with an abstract representation of the type posited here. In addition, variance appears to be estimated at relatively low levels of vision (Norman, Heywood, & Kentridge, 2015), with variance in one feature dimension influencing the perception of variance in others (Maule & Franklin, 2020), again supporting the possible existence of a representation indifferent to carrier.

As to the nature of parameter-space dimensions, all could in principle be entirely abstract, and treated the same way. Position, however, appears to have a special status in visual perception, its coding being involuntary and central to many representations (Cave & Pashler, 1995; Chen, 2009). As such, spatial positions may be anchored in a geometric map, with normalization limited to linear rescaling; if so, distortions of space could affect performance more severely than distortions of other carriers.

[8] Alternatively, this might be done by equalizing the ranges of the values. Since the ratio between standard deviation and range was always set to the same value (viz., 0.2) in all the stimuli here, this issue cannot be investigated using the data in this study.

Extended Entropy Theory

While parameter space can account for the similarity of correlation perception across different carriers, it does not account for their particular form, viz., eqs. (1) and (2). Given that similar representations are involved, the mechanisms involved may also be similar to each other, and similar to those used for determining correlation in scatterplots. A natural step is then to consider adapting the entropy theory originally developed for scatterplots to parameter space. Entropy theory asserts that perceived correlation is proportional to the entropy of the probability density function that describes the likelihood of an element at any two-dimensional location in space (Appendix A). This can be extended in a straightforward way to the entropy of the density function describing the likelihood of an element with a particular (one-dimensional) location and carrier value; entropy could then be determined in the same way as for scatterplots. Given the normalization and equalization processes posited here, the situation would be much the same as for scatterplots of equal horizontal and vertical extent. The result would then be performance as described by eqs. (1) and (2).[9]

Carrier Characteristics

The perception of correlation in all the stripplots examined here—as well as the scatterplots in (Rensink, 2017)—appears to be described reasonably well by eqs. (1) and (2), with performance differing only in the values of k and b. Can the values of these parameters say anything about the nature of the particular carriers involved?

[9] Another possibility might be mutual information I, a general measure of the association between random variables. For a bivariate gaussian, $I(x,y)$ is proportional to bivariate entropy $H(x,y)$, and so would give rise to the same behavior. However, $I(x,y)$ is a more derived quantity, generally being defined in terms of $H(x,y)$ and not the other way around; it is difficult to see how it could be computed without recourse to the mechanisms of the kind described here. Moreover, humans do not appear sensitive to mutual information *per se* when detecting general relationships between variables, using more limited measures instead (Fass, 2006). Entropy may be one of these measures.

Variability

According to eq. (4), variability $k = - T_C \ln(1-b)$, where $T_C > 0$ is a threshold constant. As is evident (Table 5), values for T_C within any carrier show no reliable differences across conditions. Nor does T_C differ much across the various carriers ($F(11, 228) = 1.793$; $p = .06$); average T_C = 0.16 [0.15, 0.17], suggesting that T_C is largely if not entirely independent of the carrier used,[10] with k—for a given threshold level and number of elements—essentially a function of b alone.

Note that for the case of scatterplots, eq. (4) predicts $k \approx 0.4$, far from the value of 0.21 encountered in Rensink (2017). It may be that the factor T_C for an abstract carrier must be replaced by a different factor $T_S \approx 0.09$ when both dimensions are spatial; if so, this would be further evidence of a special status for spatial position.

Carrier	Cond	k	b	Difference	T_C
Luminance	1A	0.24 *[0.18, 0.30]*	0.68 *[0.58, 0.75]*	$F(3,76) = 1.832$ $p = .149$	0.19 *[0.17, 0.20]*
	1B	0.21 *[0.15, 0.27]*	0.69 *[0.60, 0.77]*		
	1C	0.23 *[0.18, 0.27]*	0.76 *[0.68, 0.83]*		
	1D	0.29 *[0.25, 0.34]*	0.84 *[0.74, 0.91]*		
Color	2A	0.17 *[0.12, 0.21]*	0.67 *[0.57, 0.75]*	$F(2,57) = 0.301$ $p = .741$	0.15 *[0.13, 0.16]*
	2B	0.14 *[0.11, 0.18]*	0.63 *[0.52, 0.72]*		
	2C	0.27 *[0.23, 0.32]*	0.85 *[0.77, 0.90]*		
Orientation	3A	0.39 *[0.30, 0.49]*	0.90 *[0.80, 0.96]*	$F(2,57) = 0.089$ $p = .915$	0.16 *[0.14, 0.19]*
	3B	0.38 *[0.32, 0.44]*	0.90 *[0.83, 0.95]*		
	3C	0.32 *[0.25, 0.38]*	0.88 *[0.77, 0.95]*		
Size	4A	0.26 *[0.21, 0.30]*	0.83 *[0.76, 0.89]*	$F(1,38) = 0.025$ $p = .876$	0.15 *[0.13, 0.16]*
	4B	0.25 *[0.20, 0.31]*	0.82 *[0.73, 0.88]*		

[10] Omitting condition 1 A, differences are even less pronounced: $F(10,209) = 0.792$; $p = .636$.

Table 5: Values of T_C for different carriers. Values for T_C via eq. (4), using values for k and b_{disc} from Tables 1-4. For each carrier, values are similar, supporting eq. (4).

Bias

Entropy theory views bias b as reflecting the residual noise of the carrier involved. More precisely, assuming that the density function for position has a residual width w_{res} (inherent noise) about the $y = x$ axis when $r = 1$ (Figure 16a), bias can be expressed as (Appendix A, eq. A6):

$$b = 1/(1 + c^2)\,, \tag{5}$$

where $c > 0$ is proportional to the ratio of w_{res} to the standard deviation σ of the distribution. Given two values b and b', eq. (5) implies that their residual noise levels w_{res} differ by a factor

$$q = \sqrt{1/b' - 1}/\sqrt{1/b - 1}\,. \tag{6}$$

Let $\alpha > 0$ be the factor by which w_{res} is increased in the carrier dimension compared to position. The increase q in width of the area swept along a 45° angle (the $y = x$ axis) by an ellipse of axes w_{res} and αw_{res} is then (Figure 16b)

$$q = \sqrt{(1 + \alpha^2)/2}. \tag{7}$$

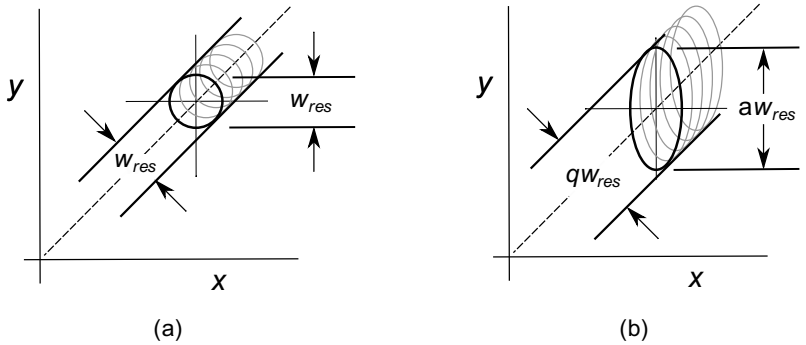

Figure 16. Residual noise. (a) Signals in both spatial dimensions have the same level of noise, corresponding to a residual width w_{res} (or variance w_{res}^2). (b) If one of the signals has a greater amount of noise (corresponding to a lengthening of the ellipse by a factor $\alpha > 0$ in the abstract dimension), the result is a residual width $q\,w_{res}$. Since the width swept out by an ellipse with axes A and B along a 45° diagonal is $\sqrt{(A^2 + B^2)/2}$, $q\,w_{res} = \sqrt{(1 + \alpha^2)/2}\,w_{res}$.

Combining eqs. (6) and (7) then yields the relative increase in noise for a given carrier:

$$\alpha = \sqrt{\frac{2/b' - 2}{1/b - 1} - 1}\,. \qquad (8)$$

The *relative efficiency* η of a carrier can be defined as its signal-to-noise ratio relative to that for position. Since (by definition) $\alpha = 1$ for position, it follows that for any given signal strength,

$$\eta = 1/\alpha. \qquad (9)$$

Using eqs. (8) and (9) with $b = 0.90$ for spatial position (Rensink, 2017), the values of α and η for various carriers follow. These are shown in Table 6.

Carrier	α	η	Levels (noise)	Levels (S-H)	Levels (obs.)	Qual. (vis.)
Luminance	2.59	0.39	4.3 [3.8, 4.9]	3.8 [3.2, 4.4]	2.7 – 4.8	Poor
Color (axis)	3.18	0.31	3.7 [3.1, 4.3]	3.1 [2.6, 3.8]	—	Poor
Color (rainbow)	1.56	0.64	6.5 [4.9, 9.5]	6.2 [4.4, 9.5]	3.1 – 9.6	Medium
Orientation	0.90	1.11	10.4 [8.0, 16.5]	10.5 [7.8, 17.2]	6.3 – 9.4	Medium-good
Size (length)	2.01	0.50	5.2 [4.1, 6.8]	4.8 [3.6, 6.5]	2.1 – 7.4	Medium
Position	1.0	1.0	—	—	9.5	Good

Table 6: Characteristics of individual carriers, relative to position. Values for α and η via eqs. (8) and (9), using values of b taken from Tables 1-4. Levels (noise): number of levels based on residual noise ($wres$), via eq. (10). Levels (S-H): number of levels based on Shannon-Hartley theorem, via eq. (11). Square brackets show 95% confidence intervals. Levels (obs): Representative numbers of observed levels of perceptual magnitude, from the references in Miller (1956), Card et al. (1999), Nizami (2010), and Ward, Grinstein, & Keim (2015), with the estimated number of bits converted to the number of levels (categories); values are plus or minus the standard deviation of the set of results. Values for color axes are not available; estimates for rainbow are based on those for two-dimensional color "hue". Part of the variability in observed values is likely due to the dependence of performance on exposure time, which differs across studies (Miller, 1956). Qual. (vis): Qualitative ratings of carrier quality from information visualization studies, based on Cleveland & McGill (1987), Ware (1988), and Roth (2017).

Complexity

The preceding discussion focused largely on single perceptual dimensions (simple features) that map to single dimensions in parameter space. The rainbow map and the mapping to circles, however, involve multiple dimensions; interestingly, the results for these generated the only effects that the proposal here does not entirely account for—viz., reliable differences between b_{disc} and b_{est}. Although a framework for multiple dimensions is beyond the scope of the current work, a few tentative observations might still be made about some of the issues involved.

To begin with, the efficiency η of a rainbow map (based on discrimination) is greater than for a color axis (Table 6). This points to a relatively low level of residual noise, suggesting that for this mapping, the red-green and blue-yellow signals are components of a compound signal of some kind. In line with this, the ratio of η for the rainbow map to that of a color axis is $0.64 / 0.31 \approx 2$, suggesting that the information in these components is added in some way. The greater signal-to-noise ratio for the rainbow map may account for the finding that it—and more generally, color mappings involving multiple dimensions—is more effective at conveying quantity than mappings that involve a single color dimensions; this may account for its popularity in visualization despite several problems in its use (Borland & Taylor, 2007; Reda &Szafir, 2021). In any event, the finding that $b_{disc} \neq b_{est}$ for the rainbow map (contrary to what is found for features like luminance and orientation) shows that not all perceptual continua give rise to exactly the same behavior. In this regard, it may be worth defining a *simple carrier* as one which follows eqs. (1) and (2) and for which $b_{disc} = b_{est}$; a *complex carrier* in contrast would be one which obeys eqs. (1) and (2), but for which the biases are not equal. The findings here would then indicate that single color dimensions are simple carriers, whereas rainbow maps, containing two such dimensions, are complex.

The results in regards to the circles (condition 4B) are consistent with this view, in that the carrier may be composed of separate width and height measures (Morgan, 2005; Raidvee et al., 2020). The efficiency η for circles in regards to estimation is greater than for line segments, consistent with the idea that the information in its constituent dimensions has been combined in some way. Interestingly, the difference between b_{disc} and b_{est} for circles goes in the opposite direction as for the rainbow map. This may be due to the dimensions involved with circles being co-ordinated, something that does not occur for the rainbow map. Alternatively, it might reflect the feature being separable or integral (i.e., its component features can or cannot be individually selected): color is a well-known integral property, whereas width and height can be separated for at least some tasks (Pramod & Arun, 2014). If the latter case, the size of the difference between b_{disc} and b_{est} may indicate the degree to which integrality or separability exists. More work on this is needed.

Connection to Channel Capacity

The ability of a visual property to convey information is often characterized via its *channel capacity*, defined as the maximum number of bits that can be effectively transmitted by the corresponding perceptual channel (Miller, 1956). Capacity can be expressed as the logarithm of the number of distinct perceptual levels (or *quantitative categories*) supported by the channel, which is governed by its signal-to-noise ratio (see e.g., Nizami, 2010). Given this, how might these estimates connect to the results for the carriers obtained here?

Perceptual Levels

To determine the number of distinct levels m in a carrier, recall that in parameter space, numerical values are mapped to a carrier space of maximum range $M > 0$, and residual noise αw_{res}. If the

average separation between distinct levels of a carrier is approximately equal to the magnitude of residual noise, the number of distinct levels will be approximately $m = M/\alpha w_{res} + 1$ (Figure 17). Taking the ratio of m to m_p (the number of distinct levels for position, where $\alpha = 1$) allows M/w_{res} to be factored out, yielding

$$m = \eta(m_p - 1) + 1. \qquad (10)$$

The resulting estimates (using $m_p = 9.5$; Miller, 1956) are shown in Table 6. These values are consistent with those encountered in classic experiments on the perceived number of levels for individual visual properties. Indeed, the relatively good match with the latter suggests that parameter-space representation may be directly involved in the perception of sensory magnitude.

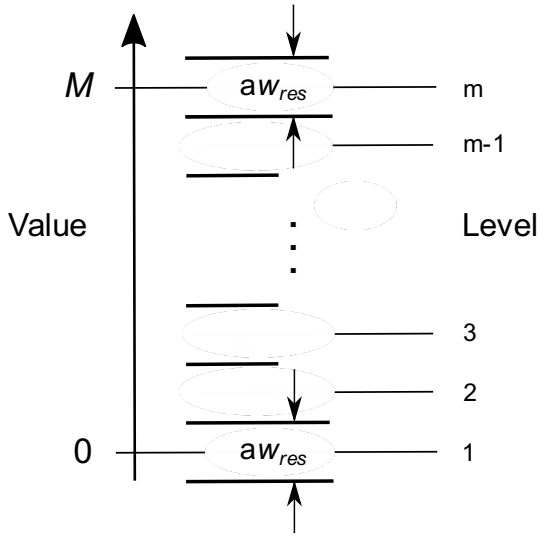

Figure 17. Number of levels as a function of residual noise. Each value is mapped to a particular quantitative category, or level; thicker lines represent category boundaries. Given a set of values normalized to range from 0 to M, each having a noise $\pm\alpha w_{res}/2$ about its average value, the number of distinct levels $m \approx R/\alpha w_{res} + 1$.

A slightly different formula for m can be obtained via the Shannon-Hartley theorem of information theory, which states that $m = \sqrt{1 + S/N}$, where S is the average signal energy, and N the energy of inherent noise (Pierce, 1980). Given that energy is proportional to the square of signal

magnitude, and N is proportional to the energy of the residual noise αw_{res}, the value of S/N for a carrier relative to that for position is η^2. Thus, again denoting the number of levels for position by m_p, the Shannon-Hartley theorem yields

$$m = \sqrt{1 + \eta^2 (m_p{}^2 - 1).} \qquad (11)$$

The results are shown in Table 6. Although the matches are not exact, the two sets of values are reasonably close to each other, as well as to the observed number of levels of absolute perceptual magnitude.

Qualitative Ratings

The estimates of residual noise w_{res} (and corresponding number of perceptual levels) obtained here are also consistent with ratings of carrier quality from work in information visualization (Table 6). In the case of luminance, for example, the estimate of about 4 levels is in line with recommendations made in the information visualization literature, where luminance is regarded a relatively poor visual variable for conveying quantitative information, useful mainly for conveying ordinal values (e.g., Bertin, 1967/2011; Cleveland & McGill, 1987; Roth, 2017).

The estimate of about 3 distinct levels for a color axis is the lowest of the carriers examined here. This is consistent with opinion in information visualization that color—at least, along these axes—should not be used to convey quantitative information, instead being confined to ordinal or even just nominal data (Roth, 2017). It is also worth noting that the estimates for both color axes are much the same, and are also not far from that for luminance. (Results consistent with this were also found by Ware, 1988). It has been suggested that color is recoded from its three-color RGB representation in the retina into three orthogonal channels of equal capacity, so as to enable efficient

transmission of information (Buchsbaum & Gottschalk, 1983); the results here support this to an extent, indicating that all three channels convey roughly similar amounts of information. In regards to the rainbow map, the finding of about 6 distinct colors falls within the range of 5–7 colors estimated from studies on isoluminant target identification (Healey, 1996); this suggests that the results for the rainbow map may be representative of mappings to various two-dimensional color (hue) spaces (cf. Reda &Szafir, 2021). Note that while the higher signal-to-noise ratio for the rainbow map does enable more quantitative levels to be discerned, it also corresponds to a greater bias, making the rainbow stripplot less suitable for accurately representing correlation.

Meanwhile, the estimate of about 10 levels for orientation is compatible with the belief in information visualization that orientation is well suited for conveying quantitative information; indeed, the results here suggest that for at least some visualization tasks, orientation may be just as useful as position. The number of estimated levels is consistent with work on visual discrimination suggesting that orientation detectors have on average a full bandwidth of 18-24° (Gheiratmand & Mullen, 2014), corresponding to about 8-10 levels. It is also compatible with work on visual search indicating that items should have a separation of about 20° on average—corresponding to 9 levels—if they are to be perceived as distinct (Wolfe, Friedman-Hill, Stewart, & O'Connell, 1992).

Finally, the estimate for size is also consistent with recommendations in information visualization, where this property is considered reasonably good for conveying detailed quantitative information (Table 6). It may be worth noting that the estimate here of about 5 levels is similar to the 4-6 size channels posited by several models of spatial vision (e.g., Wilson, McFarlane, & Phillips, 1983). It would be interesting to see if this number also manifests in other aspects of visual perception, such as texture perception or visual search.

Other Connections

Discussion to this point has focused on the issue of whether abstract quantitative information can be carried by visual features, and what might be the properties of the carriers involved . However, the results also appear to have implications for several other aspects of perception.

Perception of Number

The data from the experiments here show that perceived correlation is described by a logarithmic function—essentially Fechner's Law—at least as well as by any power function (Appendix C); this differs from the situation for simple sensory properties, where power functions are typically the best descriptors of perceived magnitude (Ross, 1997). In addition, as mentioned earlier, each JND appears to correspond to a constant number of (abstract) bits, with the value of T_C being largely indifferent to carrier (Table 5). Both these findings support the proposal that perceived correlation is not a simple sensory property, but a more abstract quantity no longer linked to the original sensory representation.

The validity of Fechner's Law for correlation perception may stem from the absence of a sensory component in the associated quantity (cf. Billock & Tsou, 2011). If so, other abstract quantities and relationships—which, incidentally, are commonly displayed in visualization—may express similar behavior. It is also worth noting that the Weber fraction for perceived number is 0.2 - 0.25 (Burr & Ross, 2008; Cheyette & Piantadosi, 2020); this value is considerably higher than those for sensory properties (Ross, 1997), but similar to the values found here for k, which is essentially a Weber fraction. This hints that an elevated Weber fraction may be another signature of an abstract—although still relatively low-level—perceptual quantity.

Other connections are also possible. For example, it has been proposed that the sense of number in high-level reasoning is based on a more basic and automatic sense of continuous magnitude that is amodal and able to integrate the outputs of different perceptual streams (Mix, Levine, & Newcombe, 2016). The origins of such a representation may lie in the parameter space proposed here. More generally, the existence of parameter space itself could provide an interesting perspective on the relationship between perception and cognition: its representations are abstract (i.e., devoid of linkages to physical properties) and thus conceptual, while the processes involved have a density typical of low-level operations that are perceptual (cf. Tacca, 2011). If a sharp divide exists between perception and cognition, on which side would parameter space fall?

Low-level Perception

The developments here may also connect with several aspects of low-level visual perception. For example, most theories of visual search posit a set of basic visual features rapidly picked up at low levels using little or no attention, with items containing a unique feature able to "pop out" to an observer (see e.g., Wolfe & Utochkin, 2019). All such features examined here—as well as position—appear to be carriers, differing only in their level of residual noise. The question then is the extent to which this holds: are all features carriers? A related issue is the converse: are all carriers features? An interesting possibility is that the set of basic visual features corresponds exactly to the set of carriers; if so, this would provide an independent way of determining whether a given visual property is a basic feature.

The proposal of a tight binding of information from different dimensions (via colocation) differs from the views of early theories of search (and related work), which asserted that features are separated at low levels of visual perception (see Treisman, 1996). However, later findings did

point to such binding—e.g., search based on features stemming from components that must be bound together correctly (e.g., Duncan, 1984; Enns & Rensink, 1991; Rensink & Enns, 1995). An interesting possibility in this regard is that such bindings exist at low levels and are used for constructive purposes (e.g., to form structures such as parameter space), but are lost in the representations used in the higher-level, conscious control of low-level processing (Rensink, 2015).

Another potential connection is with the space in which visual features are located. Most theories of search posit a geometric space (map) at early levels that collates the featural information at each location (Treisman & Gelade, 1980; Wolfe, Cave, & Franzel, 1989). The elements of parameter space are also located in a such a manifold. And given that average display times in the experiments here are on the order of a second, parameter-space descriptions may well be formed rapidly at early levels, with little or no attention. However, although (normalized) geometric dimensions are part of parameter space, the other dimensions only involve abstract values. Interestingly, the lack of direct linkage with sensory properties may explain a phenomenon that cannot be accounted for by current theories of search: why attention cannot select subsets of different colors when perceiving correlation in scatterplots (Elliott & Rensink, 2019, 2020). In the view of parameter space theory, the information that attention could use to select items in this situation—viz., a representation of the sensory color itself—is simply not there.

A related connection may also be to ensemble perception, where various statistical properties of sets of items can be rapidly determined with relatively little attention (Alvarez, 2011; Ariely, 2001; Whitney & Leib, 2018; Utochkin, 2015). In particular, the density functions posited for correlation perception may be related to the distributions thought to underlie ensemble coding: both kinds of representation are probabilistic, involve features, and can be carried out relatively rapidly (Rensink,

2014, 2017). But note that entropy theory involves the widths of density functions rather than their first or second moments. In addition, parameter-space theory asserts that these functions describe a multi-dimensional space anchored in the image, whereas ensembles generally have no such anchoring, effectively having no direct referent in space.

However, parameter space could serve as a basis for the representations thought to underlie both ensemble perception and visual search (and perhaps texture perception). In the case of search, the underlying representations could be viewed as density functions that have been summed over the abstract dimensions, allowing direct reference by position although not by value (Figure 18a). Conversely, ensembles could be viewed as marginal probability densities that have been summed over a given geometric space, able to be referenced by value but not position (Figure 18b). As such, parameter space could be viewed as a space that can—at least conceptually—link the representations underlying visual search and ensemble perception.

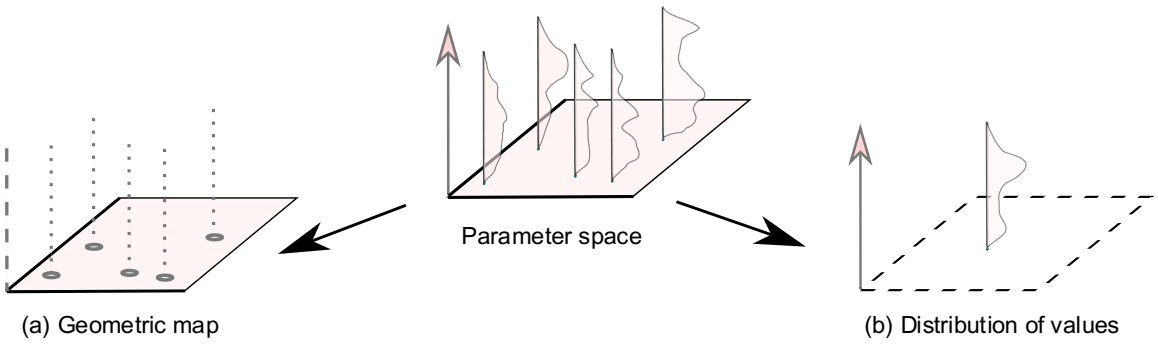

Figure 18. Possible relation of parameter space to low-level perception. Shown here is a parameter space containing two dimensions that are anchored to space and one dimension that is not. For illustrative purposes, density functions are shown only for a set of locations; in general, such functions would exist at points in space. (a) Geometric map typical of those posited as underlying visual search. Summing the information in density functions at each spatial location over the nonspatial carrier dimension yields spatial maps that reference the result for each function (e.g., its average value) by position. (b) Distribution of values underlying ensemble perception. Summing density functions over all positions of a given region of space results in a distribution of values over the nonspatial properties, with no direct reference to position.

Open Issues

Although investigation here has touched upon several aspects of visual perception, its results are more a beginning than an end. Various issues remain in regards to better understanding the nature of the phenomena encountered, as well as how they relate to perception in general. These include:

1. *Timecourse*. How quickly are correlation estimates formed? Although the results here suggest that low levels of processing are involved, it is not clear that the relevant processes are also early—i.e., low-level *and* rapid, occurring within a few hundred milliseconds of viewing. If such is the case, it would strengthen the connection of carriers to visual features, which are believed to be determined within a similar amount of time. Studying the effect of exposure time on performance would be useful here. A "basic" stage of correlation perception in scatterplots appears to be complete within c. 400 ms (Rensink, 2014); it would be interesting to see if this limit can be tightened, and whether the same limit applies to other carriers.
2. *Spatial interference*. The stripplot elements used here are relatively close to each other—typically a fraction of a degree of viewing angle. This makes them susceptible to low-level phenomena such as crowding, which pools information from nearby locations (see Keshvari & Rosenholtz, 2016). There may also be effects—at least for orientation and circles—due to the overlap of adjacent elements (cf. the relatively high JNDs for orientation). Such effects could be explored by varying the number of items and their spacing. For scatterplots, JNDs are higher when 24 or fewer dots are present (Rensink, 2014), while performance is largely unaffected for 48-200 dots. It would be interesting to know if this pattern also holds for stripplots.
3. *Attentional selection*. When perceiving correlation in a designated set of dots among a second (distractor) set, interference always exists, even when the distractor dots differ in color (Elliott & Rensink, 2019, 2020). This indicates a failure to attentionally select items on the basis of

color, Curiously, selection on the basis of color *can* be easily done when estimating mean values or the numerosity of similar stimuli (Chong & Treisman, 2005), suggesting that the failure may be specific to the perception of correlation. This phenomenon needs further exploration; Does attentional selection also fail for other visual features and other substrates—e.g., when perceiving correlation in a position-orientation stripplot, could a subset of lines fail to be selected on the basis of color? And what do such failures say about the attentional mechanisms involved?

4. *Nature of carriers*. The results here point to the existence of complex carriers containing two perceptual dimensions. But could carriers contain three dimensions, or even more? Could some involve scene-based properties, such as the three-dimensional orientation encountered in visual search (Enns & Rensink, 1991)[11], or the physical (rather than retinal) size found in ensemble perception (Haberman & Suresh, 2020)? Could some kinds of textures be carriers? More generally, could any perceptual continuum be a carrier? And could the amount of residual noise—related to bias b (eqs. (8) and (9))—of a carrier be related to the visual strength of the features involved (Huang, 2015)?
5. *Other quantitative functions*. The carriers examined here can enable a reasonably accurate perception of correlation. But what other quantitative functions might they enable? Could a scatterplot, say, allow accurate detection of nonlinear trends? If so, how well for what kinds of nonlinearities? Would other carriers yield similar performance? Such behavior may provide an additional source of insight into the processes involved.
6. *Other aspects of visual perception*. Given that the features capable of guiding visual attention may be not the same as the properties that affect grouping, texture perception, or visual

[11] Work in information visualization suggests that quantitative information can be conveyed by three-dimensional volume (Mackinlay, 1986).

distinctiveness, or the properties used in visual memory (Cheal & Lyon, 1994; Huang, 2015; Wolfe & Utochkin, 2019), an interesting issue is to determine which—if any—set is identical to the set of carriers. Given that carriers are those channels capable of conveying quantitative information in the manner described here, what other subsets might be identified, and on what functional grounds? How many different aspects might there be, and how might they be related to each other? As well as casting additional light on the nature of low-level visual perception, investigation into this issue would also help clarify why different visual properties appear to be best for different tasks in information visualization (Garlandini & Fabrikant, 2009; Mackinlay, 1986; McColeman, Yang, Brady, & Franconeri, 2021)?

7. *Role of abstraction*. Another issue to consider is why abstract quantities are represented in the first place: why not simply use sensory properties for grouping and attentional selection, say, and leave it at that? It is suggested here that abstraction enables information from different carriers to be combined. But is this the only reason? A related issue: where does the decoding into purely abstract quantity occur? Is this during the formation of parameter-space representations? Or might it perhaps occur earlier? An important challenge is to determine the extent to which abstract (vs. sensory-linked) quantities are involved in various kinds of perceptual processing, and why this might be.

Conclusions

This study has shown that the features of luminance, color, orientation, and size all support the perception of correlation between values represented by their sensory magnitude and values represented by their spatial position. This suggests that the information in these features can exist in an abstract form—one with no linkage to the original sensory properties (other than the level of

inherent noise)—which enables information from different perceptual dimensions to be combined. And given that correlation can be perceived when viewing stripplots containing a large number of elements, the information from these dimensions is likely bound in a dense fashion, at relatively low levels of vision.

Another finding is that perception is much the same for various kinds of stripplot, as well as for scatterplots, suggesting that the features tested are all *carriers*—properties capable of conveying quantitative information in the same way as spatial position. This can be accounted for via *parameter space theory*, which posits a common abstract manifold in which the information about individual elements can be represented via their location in this space. The specific form of these laws can be accounted for by extending the entropy theory developed for scatterplots to this space, via the proposal of a probability density function describing the joint distribution of the values involved. Performance is consistent with perception being that of the entropy (disorder) of this function; the particular behavior for each carrier appears largely due to the amount of residual noise it contains. The estimates of these noise levels are broadly compatible with those found in classic work on absolute perceptual judgment (Miller, 1956).

These results provide a new perspective on the nature of visual perception, particularly in regards to the low-level processing believed to underlie tasks such as ensemble perception and visual search, as well as the representation of abstract quantities. It remains to be seen how far this perspective can take us. Meanwhile, the results here make a case for the productive interaction of the areas of vision science and information visualization, using phenomena encountered in visualization as inspiration for research in vision science. Not only can this kind of research enable important aspects of information visualization be put on firmer foundations, but the results can also

give us interesting new insights into the nature of the visual intelligence that helps us makes sense of our world (Rensink, 2017, 2021b).

Context of the Research

The ideas here originated as part of a research program investigating why effective visualization systems are effective—what aspects of our visual intelligence do they draw upon? The general approach of this program is to consider the graphical representations in visualization systems as stimuli in their own right, and investigate accordingly. Such work can potentially uncover new aspects of perception (such as the entropy theory mentioned here), as well as provide a theoretical grounding for several aspects of information visualization itself (see Rensink, 2021b).

Their initial focus of this program has been on the perception of correlation, a quantity used in real-world analysis that is relatively easy to isolate. Initial work examined the perception of correlation in scatterplots, a real-world design that can be manipulated in many ways. This study continues that approach, extending it to properties beyond position. The results here would seem to justify investigations of this kind. Several possible avenues to explore in the near future are discussed in the Open Issues section; these include investigations of the nature of carriers, as well as the effects of timing and the number of elements. Further in the future, investigation might focus on other issues related to visualization, such as the perception of outliers and the perception of clusters, two other tasks for which scatterplots are commonly used. More generally yet, it may also be worth considering yet other kinds of visualization designs, which could enable us to uncover even more aspects of our visual intelligence.

References

Alvarez, G. A. (2011). Representing multiple objects as an ensemble enhances visual cognition. *Trends in Cognitive Sciences*, **15**: 122–131.

Ariely, D. (2001). Seeing sets: Representation by statistical properties. *Psychological Science*, **12**: 157–162.

Ben-Naim, A. (2008). *A Farewell to Entropy: Statistical Thermodynamics Based on Information*. London: World Scientific.

Bertin, J. (1967/2011). *Semiology of graphics: Diagrams, networks, maps*. (Translator W.J. Berg). Redlands CA: Esri Press.

Billock, V.A., & Tsou, B.H. (2011). To honor Fechner and obey Stevens: Relationships between psychophysical and neural nonlinearities. *Psychological Bulletin*, **137**: 1-18.

Borland, D., & Taylor, R. M. II. (2007). Rainbow color map (still) considered harmful. *IEEE Computer Graphics and Applications*, **27**:14-17.

Buchsbaum, G., & Gottschalk, A. (1983). Trichromacy, opponent colours coding and optimum colour information transmission in the retina. *Proc. Royal Society London*, **B 220**: 89-113.

Burnham, K. P. & Anderson, D. R. (2002). *Model Selection and Multimodel Inference: A Practical Information-Theoretic Approach* (2nd ed.). New York: Springer.

Burr, D., and Ross, J. (2008). A visual sense of number. *Current Biology*, **18**: 425–428.

Card, S.K., Mackinlay, J.D., & Shneiderman, B. (1999). Information visualization. In Card, S.K., Mackinlay, J.D., & Shneiderman, B. (Eds.) *Readings in Information Visualization: Using Vision to Think*, chs. 1 & 6. San Francisco: Morgan Kaufman.

Carnap, R. (1966). In M. Gardner (Ed.), *An Introduction to the Philosophy of Science* (pp. 70-77). New York: Basic Books.

Cavanagh, P., Arguin, M., & von Grünau, M. (1989). Interattribute apparent motion. *Vision Research*, **29**: 1197–1204.

Cave, K. R., & Pashler, H. (1995). Visual selection mediated by location: Selecting successive visual objects. *Perception & Psychophysics*, **57**: 421-432.

Cheal, M., & Lyon, D. R. (1994). Allocation of attention in texture segregation, visual search, and location-precuing paradigms. *The Quarterly Journal of Experimental Psychology*, **47**: 49-70.

Chen, Z. (2009). Not all features are created equal: Processing asymmetries between location and object features. *Vision Research*, **49**: 1481-1491.

Cheyette, S.J. & Piantadosi, S.T. (2020). A unified account of numerosity perception. *Nature Human Behaviour,* **4**: 1265–1272.

Chong, S.C., & Treisman, A. (2005). Statistical processing: computing the average size in perceptual groups. *Vision Research*. **45**: 891–900.

Cleveland, W.S., Diaconis, P., & McGill, R. (1982). Variables on scatterplots look more highly correlated when scales are increased. *Science*, **216**: 1138-1141.

Cleveland, W.S., & McGill, R. (1987). The visual decoding of quantitative information on graphical displays of data. *Journal of the Royal Statistical Society A*, **150**: 192-229.

Cumming, G. (2012). *Understanding the new statistics: Effect sizes, confidence intervals, and meta-analysis*. New York: Routledge.

Doherty, M.E., Anderson, R.B., Angott, A.M., & Klopfer, D.S. (2007). The perception of scatterplots. *Perception & Psychophysics*, **69**: 1261-1272.

Duncan, J. (1984). Selective attention and the organization of visual information. *Journal of Experimental Psychology: General*, **113**: 501-517.

Elliott, M., & Rensink, R. (2020). Further evidence that probability density shape is a proxy for correlation. *Journal of Vision,* **20:** 1481. https://doi.org/10.1167/jov.20.11.1481. Vision Sciences Society, virtual conference, June 2020.

Elliott, M., & Rensink, R. (2019). Attentional color selection depends on task structure. *Journal of Vision,* **19:** 270b, https://doi.org/10.1167/19.10.270b. Vision Sciences Society, St. Petersburg, FL, USA, May 2019.

Enns, J.T., & Rensink, R.A. (1991). Preattentive recovery of three-dimensional orientation from line drawings. *Psychological Review*, **98**: 335-351.

Fass, D.M. (2006). Human Sensitivity to Mutual Information. PhD Thesis, Graduate Program in Psychology, The State University of New Jersey, New Brunswick, New Jersey, USA.

Faul, F., Erdfelder, E., Lang, A.-G., & Buchner, A. (2007). G*Power 3: A flexible statistical power analysis program for the social, behavioral, and biomedical sciences. *Behavior Research Methods*, **39**: 175–191.

Garlandini, S., & Fabrikant, S.I. (2009). Evaluating the effectiveness and efficiency of visual variables for geographic information visualization. In Hornsby K.S., Claramunt C., Denis M., Ligozat G. (eds) *Spatial Information Theory*. COSIT 2009. *Lecture Notes in Computer Science*, **5756**. Berlin: Springer.

Gheiratmand, M., & Mullen, K.T. (2014). Orientation tuning in human colour vision at detection threshold. *Scientific Reports*, **4**: 4285. doi: 10.1038/srep04285.

Haberman, J., & Suresh, S. (2020). Ensemble size judgments account for size constancy. *Attention, Perception, & Psychophysics,* **83**: 925–933.

Harris, R. L. (1999). *Information Graphics: A Comprehensive Illustrated Reference*. Oxford, UK: Oxford University Press.

Harrison, L., Yang, F., Franconeri, S., & Chang, R. (2014). Ranking visualizations of correlation using Weber's law. *IEEE Transactions on Visualization and Computer Graphics*, **20**: 1943-1952.

Healey, C.G. (1996). Choosing effective colours for data visualization. *Proceedings of the 7th IEEE Conference on Visualization*. pp. 263-270.

Huang, L. (2015a). Visual features for perception, attention, and working memory: Toward a three-factor framework. *Cognition*, **145**: 43-52

Keshvari, S., & Rosenholtz, R. (2016). Pooling of continuous features provides a unifying account of crowding. *Journal of Vision,* **16**: 39.

Kirk, R.E. (1995). *Experimental Design: Procedures for the Behavioral Sciences* (3rd edition). Boston: Brooks-Cole. pp. 37-40.

Kane, D. & Bertalmio, M. (2016). System gamma as a function of image- and monitor-dynamic range. *Journal of Vision*, **16**(6):4, 1–13.

Kasai, T., Morita, H., & Kumada, T. (2007). Attribute-invariant orientation discrimination at an early stage of processing in the human visual system. *Vision Research*, **47**:203-209.

Lane, D.M., Anderson, C.A., & Kellam, K.L. (1985). Judging the relatedness of variables: The psychophysics of covariation detection. *Journal of Experimental Psychology: Human Perception and Performance*, **11**: 640-649.

Mackinlay, J. (1986). Automating the design of graphical presentations of relational information. *ACM Transactions on Graphics*, **5**: 110-141.

Marr, D. (1982). *Vision: A Computational Investigation into the Human Representation and Processing of Visual Information*. San Francisco: W.H. Freeman.

Maule, J., & Franklin, A. (2020). Adaptation to variance generalizes across visual domains. *Journal of Experimental Psychology: General,* **149**: 662–675

McColeman, C.M., Yang, F., Brady, T.F., & Franconeri, S. (2021) Rethinking the ranks of visual channels. *IEEE Transactions on Visualization and Computer Graphics*, doi: 10.1109/TVCG.2021.3114684

Meyer, J. & Shinar, D. (1992). Estimating correlations from scatterplots. *Human Factors*, **34**: 335-349.

Miller, G. (1956). The magical number seven, plus or minus two: Some limits on our capacity for processing information. *Psychological Review*, **63**: 81–97.

Mix, K.S., Levine, S.C. & Newcombe, N.S. (2016). Development of quantitative thinking across correlated dimensions. In: *Continuous Issues in Numerical Cognition*, ed. A. Henik, pp. 1–33. Elsevier.

Morgan, M.J. (2005). The visual computation of 2-D area by human observers. *Vision Research*, **45**: 2564–2570.

Nizami, L. (2010). Interpretation of absolute judgments using information theory: Channel capacity or memory capacity? *Cybernetics & Human Knowing,* **17**: 111–155.

Norman, L.J., Heywood, C.A., & Kentridge, R.W. (2015). Direct encoding of orientation variance in the visual system. *Journal of Vision*, **15**: 3, 1–14.

Pierce, J.R. (1980). *An Introduction to Information Theory: Symbols, Signals & Noise*. Ch. 8. Mineola NY, USA: Dover Publications

Pramod, R.T., & Arun, S.P. (2014). Features in visual search combine linearly. *Journal of Vision*, **14**(4): 6.

Raidvee, A., Toom, M., Averin, K., & Allik, J. (2020). Perception of means, sums, and areas. *Attention, Perception, & Psychophysics*, **82**: 865–876.

Reda, K., & Szafir, D.A. (2021). Rainbows revisited: Modeling effective colormap design for graphical inference. *IEEE Transactions on Visualization and Computer Graphics*, **27**: 1032-1042.

Rensink, R.A. (2014). On the prospects for a science of visualization. In W. Huang (Ed.), *Handbook of Human Centric Visualization*. New York: Springer. pp. 147–175.

Rensink, R.A. (2015). A function-centered taxonomy of visual attention. In P. Coates and S. Coleman (Eds.), *Phenomenal Qualities: Sense, Perception, and Consciousness*. Oxford: University Press. pp. 347-375.

Rensink, R.A. (2017). The nature of correlation perception in scatterplots. *Psychonomic Bulletin & Review,* **24**(3): 776-797.

Rensink, R.A. (2021a). Data for: Visual features as carriers of abstract quantitative information. https://osf.io/2wgb7.

Rensink, R.A. (2021b). Visualization as a stimulus domain for vision science. *Journal of Vision*, **21**, 3. doi.org/10.1167/jov.21.8.3

Rensink, R.A., & Baldridge, G. (2010). The perception of correlation in scatterplots. *Computer Graphics Forum*, **29**: 1203-1210.

Rensink, R.A., & Enns, J.T. (1995). Preemption effects in visual search: Evidence for low-level grouping. *Psychological Review,* **102**: 101-130.

Ross, H.E. (1997). On the possible relations between discriminability and apparent magnitude. *British Journal of Mathematical and Statistical Psychology*, **50**: 187-203.

Roth, R.E. (2017). Visual variables. In D. Richardson, N. Castri. M.F. Goodchild, A.L. Kobayashki, W. Liu, & R. A. Marston (Eds.), *International Encyclopedia of Geography: People, the Earth, Environment and Technology*. Oxford: Wiley. (pp. 11). Doi: 10.1002/9781118786352.wbieg0761.

Simoncelli, E., & Olshausen, B. (2001). Natural image statistics and neural representation. *Annual Review of Neuroscience*, **24**: 1193–1216.

Smith, A.R. (1995). Gamma correction. *Microsoft Technical Memo 9*. Microsoft Corporation.

Spence, R. (2014). *Information Visualization: An Introduction*. New York: Springer.

Stevens, S.S. (1966). Duration, luminance, and the brightness exponent. *Perception & Psychophysics,* **66:** 96–100.

Stone, J.V. (2015). *Information Theory: A Tutorial Introduction*. Sebtel Press.

Tacca, M. C. (2011). Commonalities between perception and cognition. *Frontiers in Psychology*, **2**: 358. doi: 10.3389/fpsyg.2011.00358,

Treisman, A. (1996). The binding problem. *Current Opinion in Neurobiology*, **6:** 171-178.

Treisman, A. & Gelade, G. (1980). A feature-integration theory of attention. *Cognitive. Psychology,* 12: 97–136.

Turatto, M. & Galfano, G. (2000). Color, form and luminance capture attention in visual search. *Vision Research*, **40**: 1639-1643.

Utochkin, I.S. (2015). Ensemble summary statistics as a basis for rapid visual categorization. *Journal of Vision*, **15**: 8. doi: https://doi.org/10.1167/15.4.8.

Ward, M.O., Grinstein, R., & Keim, D. (2015). *Interactive Data Visualization: Foundations, Techniques, and Applications* (2nd ed.), ch. 3. Boca Raton, FL: Taylor & Francis.

Ware, C. (2012). *Information Visualization: Perception for Design* (3nd ed.). New York: Morgan Kaufmann.

Ware, C. (1988). Color sequences for univariate maps: Theory, experiments and principles. *IEEE Computer Graphics and Applications*, **8**: 41-49.

Whitney, D., & Leib, A.Y. (2018). Ensemble perception. *Annual Review of Psychology***, 69:** 105-129.

Wilson, H.R., McFarlane, D.K., & Phillips, G.C. (1983). Spatial frequency tuning of orientation selective units estimated by oblique masking. *Vision Research*, **23**: 873-882.

Wolfe, J. M., Cave, K. R., & Franzel, S. L. (1989). Guided search: An alternative to the feature integration model for visual search. *Journal of Experimental Psychology: Human Perception and Performance, 15*(3), 419–433.

Wolfe, J.M., Friedman-Hill, S.R., Stewart, M.I., & O'Connell, K.M. (1992). The role of categorization in visual search for orientation. *J Exp Psychol Hum Percept Perform*. **18**: 34-49.

Wolfe, J.M. Horowitz, T.S. (2004). What attributes guide the deployment of visual attention and how do they do it? *Nature Reviews Neuroscience*, **5**: 495-501

Wolfe, J.M., Oliva, A., Horowitz, T.S., Butcher, S.J., & Bompas, A. (2002). Segmentation of objects from backgrounds in visual search tasks. *Vision Research*, **42**: 2985-3004.

Wolfe, J.M. & Utochkin, I.S. (2019). What is a preattentive feature? *Current Opinion in Psychology*, **29**: 19–26.

Appendix A – A Sketch of Entropy Theory

This appendix briefly outlines the main aspects of entropy theory as it applies to the perception of correlation in scatterplots. For details, see Rensink (2017).

The probability density function $f(x,y)\Delta x\Delta y$ of a scatterplot dot cloud specifies the probability of encountering a dot in the area $\Delta x\Delta y$ (Figure 3); for a scatterplot with n dots, the number of dots in $\Delta x\Delta y$ would be $n\,f(x,y)\Delta x\Delta y$. The scatterplots in Rensink (2017) mostly had bivariate gaussian distributions. Such distributions, centered at the origin with standard deviation σ and correlation r, have a probability density function

$$f(x,y) = \frac{e^{-q(x,y)}}{2\pi\,\sigma^2(1-r^2)^{1/2}} \qquad \text{(A1)}$$

where

$$q(x,y) = \frac{x^2-2rxy+y^2}{2\sigma^2(1-r^2)}\,. \qquad \text{(A2)}$$

The set of points at a constant fraction of the height of $f(x,y)$ can be expressed as e^{-K^2}, where K is a positive constant. The locations of these points form an *isofraction ellipse* $q(x,y) = K^2$ (Figure 3). The width w of this ellipse (twice its radius) is

$$w(r) = 2\sqrt{2}K\sigma\sqrt{1-r}\,. \qquad \text{(A3)}$$

Information entropy (in the Shannon sense) H is a statistical quantity that reflects the number of possible configurations for a given probability density; it is essentially a measure of dispersion or disorder of the distribution (see, e.g., Ben-Naim, 2008). For a scatterplot of n dots with a gaussian distribution of correlation r,

$$H(r) = An\,ln\,(2\pi\sigma^2\sqrt{1-r^2}) + B, \qquad \text{(A4)}$$

where *A* and *B* are constants. This can be approximated fairly well by $H'(r)=An\ ln\ (2\pi\sigma^2\sqrt{1-r})$ + *B'*, where *A* and *B'* are constants. If *H'* is proportional to perceived correlation *g(r)*, application of eq. (A3) results in

$$g(r) = C\ ln(w(r)) + D$$

for constants *C* and *D*. Rreplacing *w(r)* via eq. (A3) then yields

$$g(r) = C\ ln(1-br) + D' \qquad \text{(A5)}$$

for constants *b, C,* and *D'*. The term $0 < b < 1$ is introduced to account for the residual noise w_{res} caused by perceptual noise and blurring. This prevents divergence of the logarithm as *r* approaches 1 and the width of the isofraction ellipse approaches zero (Figure 16); it essentially sets the upper limit of entropy for a given carrier. It can be expressed (Rensink, 2017) as

$$b = \frac{1}{c^2 + 1}, \qquad \text{(A6)}$$

where

$$c = w_{res}/2\sqrt{2}K\sigma. \qquad \text{(A7)}$$

The other two constraints are those of calibration, viz., setting $g(0) = 0$ and $g(1) = 1$. Applying these to eq. (A5) results in the form used in the main body of the text, viz., eq. (2).

The fractional height e^{-K^2} can be determined by noting that the scatterplots in Rensink (2017) had a range of 5σ in each dimension, yielding $m = 5\sigma/w_{res} + 1$ distinct positions. Eliminating σ/w_{res} in this formula via eq. (A7) and rearranging terms, it follows that

$$K = 5\ /\ (2\sqrt{2}\ c\ (m-1)). \qquad \text{(A8)}$$

For position, $m = 9.5$ and $b = 0.90$ ($c = 0.33$), yielding $K = 0.63$, and the fraction 0.67. For $r = 0$, *f(x,y)* is a symmetric gaussian with isofraction circle of radius $\sqrt{2}\,K\sigma \approx 0.9\ \sigma$; for $r > 0$, the circle becomes an ellipse with half-width $\sqrt{2}\,K\sigma\sqrt{1-r}$ (Rensink, 2017, eq. (8)).

The estimate of this radius is close to σ, where the density function f is steepest, and so most sensitive to changes in width (and thus, r). This is also true of the ellipse: given that f is a linearly compressed version of a circularly symmetric function, the location of the steepest slope in any cross-section is not affected. This suggests a rationale for the location of the isofraction ellipse: what might be called a *principle of maximal sensitivity*. Such a principle would imply that the ellipse is defined by $\nabla^2 f = 0$, where ∇^2 operates over parameter space. (The same formula may also define luminance edges in images — see e.g., Marr, 1982). If this principle holds, estimates of m for all carriers follow without recourse to relative measures; estimates based on this (eq. (A8), with $\sqrt{2}\,K = 1$) are shown in Table A1. Most results are slightly higher than the measures based on eqs. (10) and (11). But the average difference between the measures is only 15%, suggesting that the maximum-sensitivity principle may indeed hold to at least some extent, with isofraction ellipses corresponding to much the same fraction for all carriers.

Carrier	Levels (MS)	Levels (noise)	Levels (S-H)	Levels (obs.)
Luminance	4.9 [4.4, 5.5]	4.3 [3.8, 4.9]	3.8 [3.2, 4.4]	2.7 – 4.8
Color (axis)	4.3 [3.6, 5.0]	3.7 [3.1, 4.3]	3.1 [2.6, 3.8]	—
Color (rainbow)	6.9 [5.5, 8.7]	6.5 [4.9, 9.5]	6.2 [4.4, 9.5]	3.1 – 9.6
Orientation	9.1 [7.9, 10.5]	10.4 [8.0, 16.5]	10.5 [7.8, 17.2]	6.3 – 9.4
Size (length)	5.8 [4.8, 7.2]	5.2 [4.1, 6.8]	4.8 [3.6, 6.5]	2.1 – 7.4

Table A1: Number of distinct levels in individual carriers, based on a possible maximum sensitivity principle. Levels (MS): Estimates based on maximum sensitivity principle via eq. (A8). Levels (noise): number of levels based on residual noise (w_{res}). Levels (S-H): number of levels based on Shannon-Hartley theorem. Square brackets show 95% confidence intervals. Levels for noise, Shannon-Hartley, and observed number taken from Table 6.

Appendix B – Aggregate Values

This appendix shows aggregate values for all conditions described in the main text. JNDs for discrimination include results for both directions (JND from above, JND from below); k and b_{disc} are calculated via $r_A = r + 0.5\ JND(r)$ for JND from above, and $r_A = r - 0.5\ JND(r)$ for JND from below. Also shown are the aggregate bisection values of r for subjective correlation estimates g = 1/8, 1/4, 3/8, 1/2, 5/8, 3/4, and 7/8, as outlined in the main text.

1. Experiment 1: Luminance

Condition 1A ($\gamma = 1$):

base	0.0	0.1	0.2	0.3	0.4	0.5	0.6	0.7	0.8	0.9
above	*0.30*	*0.29*	*0.27*	*0.26*	*0.23*	*0.22*	*0.22*	*0.17*	*0.12*	*0.07*
below	—	—	—	—	*0.29*	*0.31*	*0.30*	*0.24*	*0.24*	*0.17*

g (subj)	1/8	1/4	3/8	1/2	5/8	3/4	7/8
r (obj)	*0.24*	*0.41*	*0.54*	*0.68*	*0.78*	*0.85*	*0.92*

Condition 1B ($\gamma = 2$):

base	0.0	0.1	0.2	0.3	0.4	0.5	0.6	0.7	0.8	0.9
above	*0.29*	*0.25*	*0.25*	*0.21*	*0.21*	*0.20*	*0.19*	*0.14*	*0.11*	*0.07*
below	—	—	—	—	*0.23*	*0.24*	*0.23*	*0.21*	*0.19*	*0.15*

g (subj)	1/8	1/4	3/8	1/2	5/8	3/4	7/8
r (obj)	*0.23*	*0.39*	*0.53*	*0.68*	*0.76*	*0.83*	*0.91*

Condition 1C ($\gamma = 3$):

base	0.0	0.1	0.2	0.3	0.4	0.5	0.6	0.7	0.8	0.9
above	*0.26*	*0.28*	*0.22*	*0.21*	*0.24*	*0.16*	*0.17*	*0.13*	*0.11*	*0.06*
below	—	—	—	—	*0.22*	*0.22*	*0.20*	*0.18*	*0.16*	*0.11*

g (subj)	1/8	1/4	3/8	1/2	5/8	3/4	7/8
r (obj)	*0.19*	*0.38*	*0.49*	*0.65*	*0.73*	*0.84*	*0.90*

Condition 1D ($\gamma = 4$):

base	0.0	0.1	0.2	0.3	0.4	0.5	0.6	0.7	0.8	0.9
above	*0.35*	*0.27*	*0.26*	*0.25*	*0.24*	*0.19*	*0.18*	*0.15*	*0.10*	*0.06*
below	—	—	—	—	*0.27*	*0.29*	*0.23*	*0.24*	*0.20*	*0.13*

g (subj)	1/8	1/4	3/8	1/2	5/8	3/4	7/8
r (obj)	*0.24*	*0.42*	*0.57*	*0.70*	*0.78*	*0.85*	*0.91*

2. Experiment 2: Color

Condition 2A (isoluminant red-green):

base	0.0	0.1	0.2	0.3	0.4	0.5	0.6	0.7	0.8	0.9
above	*0.24*	*0.21*	*0.20*	*0.18*	*0.20*	*0.15*	*0.14*	*0.12*	*0.10*	*0.06*
below	—	—	—	*0.18*	*0.20*	*0.20*	*0.17*	*0.14*	*0.15*	*0.12*

g (subj)	1/8	1/4	3/8	1/2	5/8	3/4	7/8
r (obj)	*0.19*	*0.37*	*0.50*	*0.62*	*0.67*	*0.77*	*0.84*

Condition 2B (isoluminant blue-yellow):

base	0.0	0.1	0.2	0.3	0.4	0.5	0.6	0.7	0.8	0.9
above	*0.19*	*0.21*	*0.18*	*0.19*	*0.16*	*0.16*	*0.15*	*0.11*	*0.10*	*0.06*
below	—	—	—	*0.20*	*0.19*	*0.14*	*0.16*	*0.16*	*0.13*	*0.09*

g (subj)	1/8	1/4	3/8	1/2	5/8	3/4	7/8
r (obj)	*0.20*	*0.36*	*0.51*	*0.64*	*0.71*	*0.78*	*0.87*

Condition 2C (rainbow):

base	0.0	0.1	0.2	0.3	0.4	0.5	0.6	0.7	0.8	0.9
above	*0.29*	*0.29*	*0.25*	*0.24*	*0.22*	*0.18*	*0.14*	*0.13*	*0.09*	*0.05*
below	—	—	—	*0.24*	*0.27*	*0.23*	*0.20*	*0.17*	*0.16*	*0.12*

g (subj)	1/8	1/4	3/8	1/2	5/8	3/4	7/8
r (obj)	*0.19*	*0.37*	*0.51*	*0.65*	*0.73*	*0.83*	*0.90*

3. Experiment 3: Orientation

Condition 3A (fixed length):

base	0.0	0.1	0.2	0.3	0.4	0.5	0.6	0.7	0.8	0.9
above	*0.38*	*0.32*	*0.32*	*0.30*	*0.28*	*0.23*	*0.20*	*0.14*	*0.09*	*0.04*
below	—	—	—	—	—	*0.29*	*0.27*	*0.28*	*0.24*	*0.14*

g (subj)	1/8	1/4	3/8	1/2	5/8	3/4	7/8
r (obj)	*0.32*	*0.57*	*0.69*	*0.79*	*0.84*	*0.90*	*0.93*

Condition 3B (random length):

base	0.0	0.1	0.2	0.3	0.4	0.5	0.6	0.7	0.8	0.9
above	*0.36*	*0.31*	*0.35*	*0.28*	*0.27*	*0.21*	*0.19*	*0.14*	*0.10*	*0.05*
below	—	—	—	—	—	*0.31*	*0.28*	*0.23*	*0.19*	*0.11*

g (subj)	1/8	1/4	3/8	1/2	5/8	3/4	7/8
r (obj)	*0.34*	*0.51*	*0.67*	*0.80*	*0.86*	*0.91*	*0.95*

Condition 3C (fixed height):

base	0.0	0.1	0.2	0.3	0.4	0.5	0.6	0.7	0.8	0.9
above	*0.33*	*0.29*	*0.24*	*0.28*	*0.24*	*0.21*	*0.18*	*0.14*	*0.09*	*0.05*
below	—	—	—	—	—	*0.27*	*0.24*	*0.24*	*0.17*	*0.14*

g (subj)	1/8	1/4	3/8	1/2	5/8	3/4	7/8
r (obj)	*0.32*	*0.54*	*0.69*	*0.79*	*0.87*	*0.94*	*0.97*

4. Experiment 4: Size

Condition 4A (line length):

base	0.0	0.1	0.2	0.3	0.4	0.5	0.6	0.7	0.8	0.9
above	*0.25*	*0.28*	*0.25*	*0.25*	*0.19*	*0.16*	*0.17*	*0.12*	*0.08*	*0.05*
below	—	—	—	—	*0.26*	*0.20*	*0.21*	*0.17*	*0.12*	*0.10*

g (subj)	1/8	1/4	3/8	1/2	5/8	3/4	7/8
r (obj)	*0.22*	*0.38*	*0.54*	*0.65*	*0.76*	*0.85*	*0.92*

Condition 4B (circle diameter/area):

base	0.0	0.1	0.2	0.3	0.4	0.5	0.6	0.7	0.8	0.9
above	*0.27*	*0.23*	*0.22*	*0.22*	*0.20*	*0.16*	*0.14*	*0.12*	*0.09*	*0.06*
below	—	—	—	—	*0.25*	*0.24*	*0.23*	*0.17*	*0.16*	*0.10*

g (subj)	1/8	1/4	3/8	1/2	5/8	3/4	7/8
r (obj)	*0.36*	*0.56*	*0.67*	*0.79*	*0.85*	*0.90*	*0.94*

Appendix C – Fit of Fechner's Law

This appendix examines the best fit of aggregate correlation estimates to eight possible models; one is logarithmic (Fechner's Law), while the others are variants of the power law:

0. $g(r) = \log\ (1 - br) \,/\, \log\,(1 - b)$
1. $g(r) = \ r^a$
2. $g(r) = 1 - \sqrt{1 - r^a}$
3. $g(r) = 1 - (1 - r)^a$
4. $g(r) = br^a$
5. $g(r) = 1 - b(1 - r^a)$
6. $g(r) = 1 - b(1 - r)^a$
7. $g(r) = 1 - (1 - br)^a$

RMSE values for best fits are shown in Table B1. As is evident, the logarithmic model (Fechner's Law) provides a better fit to the data than any other law with one parameter, including the power law of the form typical of sensory magnitude perception (eq. 1; Ross, 1997). If two parameters are allowed, fits for the more complex models 5 and 7 are about 25% better.

	0	1	2	3	4	5	6	7
1A	0.0158	0.0228	0.0522	0.0345	0.0191	0.0143	0.0183	0.0154
1B	0.0188	0.0229	0.0593	0.0361	0.0218	0.0161	0.0237	0.0148
1C	0.0171	0.0246	0.0608	0.0295	0.0228	0.0156	0.0230	0.0147
1D	0.0164	0.0261	0.0506	0.0376	0.0233	0.0120	0.0240	0.0120
2A	0.0413	0.0328	0.0953	0.0543	0.0218	0.0328	0.0382	0.0138
2B	0.0318	0.0240	0.0827	0.0468	0.0200	0.0233	0.0318	0.0138
2C	0.0160	0.0212	0.0637	0.0314	0.0205	0.0118	0.0234	0.0107
3A	0.0287	0.0416	0.0379	0.0535	0.0385	0.0115	0.0377	0.0171
3B	0.0189	0.0425	0.0254	0.0399	0.0320	0.0255	0.0213	0.0211
3C	0.0123	0.0458	0.0161	0.0368	0.0281	0.0177	0.0177	0.0236
4A	0.0105	0.0229	0.0532	0.0283	0.0179	0.0115	0.0172	0.0128
4B	0.0310	0.0300	0.0362	0.0560	0.0264	0.0127	0.0274	0.0261
Avg.	**0.0215**	**0.0298**	**0.0528**	**0.0404**	**0.0244**	**0.0171**	**0.0253**	**0.0163**

Table B1: RMSE values for the best fits for each model to the data. RSS (Residual sum of squares) values are the square of these times 7.

To account for the number of degrees of freedom, the Akaike Information Criterion (AIC) is used (Burnham & Anderson, 2002); AIC = $2K + n \ln((2\pi RSS/n) + 1)$, where K is the number of parameters, and n the number of data points fit in the model. The lower the value of AIC, the better the fit. Results are shown in Table B2. As is evident, the logarithmic model still has an AIC value greater than those for power functions 5 and 7, but the difference is relatively small.[12]

	0	1	2	3	4	5	6	7
1A	-36.19	-31.07	-19.47	-25.26	-31.54	-35.56	-32.12	-34.55
1B	-33.76	-30.98	-17.68	-24.63	-29.72	-33.98	-28.52	-35.08
1C	-35.09	-29.99	-17.35	-27.47	-29.06	-34.39	-28.93	-35.17
1D	-35.71	-29.20	-19.91	-24.07	-28.74	-38.02	-28.36	-38.10
2A	-22.75	-25.96	-11.05	-18.92	-29.71	-23.97	-21.85	-36.11
2B	-26.39	-30.36	-13.03	-20.99	-30.88	-28.76	-24.40	-36.06
2C	-35.99	-32.06	-16.70	-26.59	-30.52	-38.33	-28.69	-39.64
3A	-27.86	-22.66	-23.94	-19.13	-21.75	-38.61	-22.03	-33.08
3B	-33.72	-22.35	-29.54	-23.23	-24.34	-27.51	-30.01	-30.17
3C	-39.70	-21.32	-35.97	-24.37	-26.13	-32.65	-32.60	-28.60
4A	-41.98	-30.99	-19.22	-28.05	-32.43	-38.64	-33.03	-37.14
4B	-26.78	-27.21	-24.61	-18.50	-27.00	-37.30	-26.51	-27.16
Avg.	**-32.99**	**-27.85**	**-20.71**	**-23.43**	**-28.48**	**-33.98**	**-28.09**	**-34.24**

Table B2: AIC values for the best fits of each model to the data.

For a univariate function fit by a small number of points (as is the case here), a more accurate form is AICc = AIC + *penalty*(*K*), where *penalty*(*K*) is a positive term that discourages overfitting. Although *penalty*(*K*) differs for different models, it increases with the number of degrees of freedom *K*. As such, estimates for two-parameter models (such as models 5 and 7) would be raised more than for one-parameter models. This would reduce the difference even further, if not reverse it outright. As such, the fit of Fechner's Law to the data here would seem at least comparable to that for any reasonable variant of a power law.

[12] Assuming that the conditions tested here are representative, the AIC values for the three functions have confidence intervals which overlap substantially: [-29.57, -36.41], [-31.10, -36.86], and [-31.99, -36.49], respectively.